Dinocyst assemblage constraints on oceanographic and atmospheric processes in the Eastern Equatorial Atlantic over the last 44 ky

Hardy William [(a)] *, **Penaud Aurélie** [(a)] *, **Marret Fabienne** [(b)], **Bayon Germain** [(c)], **Marsset Tania** [(c)], **Droz Laurence** [(a)]

(a) UMR 6538 Domaines Océaniques, IUEM-UBO, F-29280 Plouzané, France.

(b) School of Environmental Sciences, University of Liverpool, Liverpool, L69 7ZT, UK

(c) IFREMER, UR Géosciences Marines, BP 70-29280 Plouzané, France

*Corresponding author. Tel.: +33-298-498-741; fax: +33-298-498-760

E-mail address: william.hardy@univ-brest.fr

ABSTRACT

A new 44 ky-long record of dinoflagellate (phytoplanktonic organisms) cysts (dinocysts) is presented from a marine sediment core collected on the Congolese margin with the aim to reconstruct past hydrological changes of the Equatorial Eastern Atlantic Ocean since Marine Isotopic Stage 3. Our high-resolution dinocyst record indicates that significant temperature and moisture variations occurred across the glacial period, the Last Deglaciation and the Holocene. The use of specific dinocyst taxa, indicative of fluvial, upwelling and Benguela Current past environments for instance, provides insights into the main forcing mechanisms controlling paleohydrological changes at orbital timescales. In particular, we are able, for the last 44 ky, to correlate fluvial-sensitive taxa to monsoonal mechanisms related to precession minima / obliquity maxima combinations. While upwelling mechanisms appear as the main drivers for dinoflagellate productivity during MIS 2, dissolved nutrient-enriched Congo River inputs to the ocean also played a significant role in promoting dinoflagellate productivity between approximately 15.5 and 5 ka BP. Finally, this high resolution dinocyst study permits to precisely investigate the sub-orbital timing of the last glacial-interglacial termination including an atypical warm and wet oceanic LGM signature, northern high latitude abrupt climate change impacts in the Equatorial Eastern Atlantic, as well as a two-steps decrease in moisture conditions during the Holocene at around 7-6 and 4-3.5 ka BP.

KEYWORDS: Dinoflagellate cysts; Congolese margin; Deglaciation; Holocene; Paleoproductivity; Monsoon dynamics

1. INTRODUCTION

Reconstructions of Late Quaternary and Holocene paleoceanographic changes at the Western African margin and associated Benguela upwelling system have identified orbital and sub-orbital controls on sea-surface and continental environmental conditions (Holzwarth et al., 2007). More specifically, several palynological studies carried out in the Equatorial Eastern Atlantic Ocean, combining analysis of pollen grains and cysts of dinoflagellates (dinocysts), have provided a wealth of information on land-sea interactions in the intertropical region, through investigation of sea-surface and terrestrial vegetation changes over the last climatic cycles (Shi et al., 1998; Marret and Zonneveld, 2003; Dupont and Behling, 2006; Marret et al., 2008; Kim et al., 2010; Bouimetarhan et al., 2012; Marret et al., 2013). However, these above-mentioned studies mainly focused on the comparison between periods of extreme climatic conditions, such as the Last Glacial Maximum (Mix et al., 2001) and the Holocene Climatic Optimum, showing that higher primary productivity conditions occurred during glacial periods in response to an increase of upwelling activity while enhanced freshwater discharges from the continent occurred during interglacials. In comparison, the Last Deglaciation period, which consisted in a shift from upwelled cold waters (associated with dry conditions on land - glacial) to monsoonal regimes (associated with warm waters offshore - interglacial), has been less studied and its timing in this area remains poorly defined, mainly due to a lack of high-resolution investigations.

In this study, we have investigated a marine sediment core (KZAI-01) recovered during the ZaiAngo I cruise (Savoye et al., 2000) at the West-African continental slope, upstream the Congo deep-sea fan. This core is characterized by a high average sedimentation rate (about 25 cm/ky, maximum of 50 cm/ky) that enables high-resolution paleoenvironmental records for the last 44 ky (Bayon et al., 2012). We combined here new dinocyst data with a set of already published geochemical data for sediment provenance and weathering proxies (Bayon et al.,

2012). The comparison between terrestrial and marine proxy data can then be used to discuss about the links between environmental changes that have occurred in the Congo catchment area and past sea-surface oceanographic through dinoflagellate productivity variations.

Several objectives have motivated this study:

1) To document the potential of dinocysts for reconstructing sea-surface environments in the Eastern Atlantic Ocean and discussing about the links between continental and hydrological changes over the last 44 ky
2) To discuss orbital forcing impacts in our recorded dinocyst observations and the potential influence of the monsoonal activity on sea-surface past conditions
3) To precisely characterize, in the Equatorial Atlantic Ocean, the timing of the Last Deglaciation at a millennial time-scale resolution.

2. ENVIRONMENTAL CONTEXT ON THE CONGOLESE MARGIN

The Congo River drains the second largest catchment area of the world with a total surface of 3,600,000 km² and a mean flow of 41,000 m^3/s. This river feeds the Congo deep-sea fan (Babonneau et al., 2002; Droz et al., 2003; Savoye et al., 2009; Picot et al., 2016), one of the largest deep-sea fans in the world, *via* a submarine Pliocene canyon (Anka et al., 2009) still active at present (Heezen and Hollister, 1964; Khripounoff et al., 2003).

2.1. Present-day atmospheric context

Climatic patterns in the Congo Basin are controlled by the seasonal latitudinal migration of the Tropical Rainbelt (TR, Figure 1), which is associated offshore with high sea-surface temperatures (SST) and low salinities (Zarriess and Mackensen, 2010; Arbuszewski et al., 2013). This low pressure belt is characterized by moist air ascension and large tropical rainstorms, generated by the association of the Tropical and African Easterly Jets in the

Northern Hemisphere (Nicholson, 2009). The TR and the Inter Tropical Convergence Zone (ITCZ) constitute the complex convective system of the African monsoon system which shifts seasonally from a northward position during boreal summer to a southward position during boreal winter (Hsu and Wallace, 1976). While the central part of the Congo Basin is characterized by an equatorial regime, its northern and southern parts alternate between wet and dry seasons (Prance, 1984; Leroux, 2001). This results in a latitudinal distribution of the vegetation from rainforests to savannahs across the whole Basin (Prance, 1984). Easterly winds from the Indian Ocean also brings moisture to the Congo Basin, in particular during the austral summer, due to the presence of the Congo Air Boundary convergence zone (CAB, Tierney et al., 2011), also evidencing the influence of the eastern African monsoon system in central Africa.

2.2. Present-day oceanographic context

Surface water masses from the Congolese margin are largely influenced by the Angola Current (AC; Figure 1), a clockwise subequatorial gyre located above the north-eastern part of the Subtropical Gyre (Lass and Mohrholz, 2008). The warm waters of the AC meet the cool waters of the couple Benguela Current and Coastal Benguela Current (BC and cBC; Figure 1) at around 16°S at the Angola Benguela Front (ABF; Lass and Mohrholz, 2008). Cool surface currents cause weak evaporation and aridity conditions on the adjacent continent (Gordon et al., 1995), as well as water mass stratification on the continental shelf, itself depleted in oxygen (Gordon et al., 1995).

The South Atlantic Anticyclone, driving the Subtropical Gyre, generates SE trade winds on the SW African margin, and consequently upwelling cells throughout the BC (Gordon et al., 1995; Lass and Mohrholz, 2008). These upwelled waters bring deep nutrient-rich waters that promote high primary productivity in surface waters. The Benguela upwelling system is

114 limited northward around the ABF location (Jansen et al., 1996; Lass and Mohrholz, 2008).
115 Congo River freshwater discharges also exert an influence on the regional oceanographic
116 setting, in particular because of the relative weakness of the Coriolis force near the equator
117 that allows river plumes to extend far from the coast (da Cunha and Buitenhuis, 2013). This
118 mechanism also contributes to enhanced fluvial upwelling and thus to additional nutrients
119 exported to surface waters. Today, rainforests prevent active erosion of soils and therefore the
120 delivery of substantial fluvial nutrient supplies to the Gulf of Guinea.
121
122 **3. MATERIAL AND METHODS**
123 ***3.1. Stratigraphy of core KZAI-01***
124 Core KZAI-01 (5°42.19'S; 11°14.01'E; 816 m water depth; 10.05 m length; Figure 1) was
125 recovered during the 1998 ZaiAngo 1 cruise aboard the *Atalante* (Savoye, 1998).
126 The first published age model of core KZAI-01 (Bayon et al., 2012) was derived from seven
127 AMS ^{14}C dates on carbonates (bulk planktonic foraminifera or mixed marine carbonates;
128 Table 1), and two age constraints obtained by tuning core KZAI-01 to core GeoB6518-1
129 (well-dated sedimentary record from the nearby area; Figure 1) (Bayon et al., 2012).
130 In this study, three new AMS ^{14}C dates on planktonic foraminifera and bivalves have been
131 added between 370 and 620 cm (Table 1) in order to obtain a more robust stratigraphy for the
132 Last Glacial period (Figure 2). We have also added three new age constraints by tuning core
133 KZAI-01 to nearby well-dated core GeoB6518-1 (AMS ^{14}C dates on monospecific
134 foraminifera; Schefuß et al., 2005; Figure 2). This enables us to strengthen the chrono-
135 stratigraphy of the study core for the Early Holocene as well as for the base of KZAI-01 core,
136 not constrained by AMS ^{14}C dates below 851 cm.
137 All radiocarbon dates were calibrated to calendar ages with the Calib 7.0 program (Stuiver
138 and Reimer, 1993) associated with a 400 years correction for the marine age reservoir

(Reimer et al., 2013), and the final age model was built through linear regression between all stratigraphic pointers (Figure 2). Mean calculated sedimentation rates are around 25 cm/ky.

3.2. Palynological analysis

3.2.1. Laboratory procedure for dinocyst extraction

In this study, 203 samples were analysed for the period covering the last 44 ky with a 5 cm sampling interval (mean resolution analysis of about 200 years throughout the core, ranging between 20 and 800 years, according to the established age model). The preparation technique for palynological analysis followed the procedure described in Marret et al. (2008). Calibrated tablets of known concentrations of *Lycopodium clavatum* spores were added to each sample before chemical treatments in order to estimate palynomorph concentrations (number of dinocysts/cm^3 of dry sediments), and chemical and physical treatments included cold HCl (10%), cold HF (40%), and sieving through a single use 10 µm nylon mesh screen. The final residue was mounted between slide and coverslip with glycerine jelly coloured with fuschin. When the recommended number of 300 dinocysts could not be reached, a minimum of 100 specimens was counted on each sample (Fatela and Taborda, 2002), using a Leica DM 2500 microscope at ×630 magnification. Fifteen samples, containing less than 100 specimens, were excluded from dinocyst results. Dinocyst concentrations were based on the marker grain method (de Vernal et al., 1999) and dinocyst assemblages were described by the percentages of each species calculated on the basis of the total dinocyst sum including unidentified taxa and excluding pre-Quaternary specimens. In addition to dinocyst counts, freshwater microalgae *Pediastrum* and *Concentricystes* were also identified and counted so as to discuss river discharge intensifications in parallel with our dinocyst data.

164 *3.2.2. Dinocysts as potential tracers for past primary productivity changes*

165 Paleoproductivity regimes in the Equatorial Ocean could be inferred from our fossil
166 assemblages thanks to the transfer function based on the Modern Analogue Technique (MAT;
167 Guiot and de Vernal, 2007) developed for the Tropical Atlantic Ocean (n=208 modern
168 analogues; Marret et al., 2008). A detailed discussion of limitations and pitfalls of inferring
169 paleoproductivity from dinocyst assemblages in the study area will be discussed in a separate
170 paper. In the present study, we only focus on the dinoflagellate phytoplanktonic component
171 through past dinocyst specific observations. Indeed, among dinocyst assemblages, it is
172 possible distinguishing between cysts formed by dinoflagellates with a strict nutritional
173 strategy based on heterotrophy that we will refer as "heterotrophic cysts", and other cysts
174 formed by dinoflagellates for which the nutritional strategy can be complex involving either
175 autotrophy, heterotrophy or mixotrophy and that we will refer as "non heterotrophic cysts".
176 Relative abundances of total heterotrophic cysts have previously been used as a signal for
177 dinoflagellate primary productivity, and indirectly for marine productivity, considering that
178 heterotrophic dinoflagellates mainly feed on marine micro-organisms including other
179 dinoflagellates (whatever their nutritional strategies), diatoms and other micro-algae (e.g
180 Zonneveld et al., 2013).

181

182 **4. DINOCYST RESULTS ON CORE KZAI-01**

183 ***4.1 Dinocyst concentrations***

184 A total of 53 dinocyst taxa (Appendix) have been identified in the studied samples, with an
185 average of 15 taxa for each sample (Figure 3). Dinocyst concentrations in sediments are
186 generally very low, from 100 cysts/cm^3 to 12,000 cysts/cm^3 (Figure 3). These low
187 concentrations in the study area are thought to be caused by a strong dilution of the organic
188 matter by terrigenous inputs (cf. Figure 3) with a clear negative correlation between maximal

189 values of terrestrial inputs (Ti/Ca and minimal values of dinocyst concentrations), and also a
190 probable competition with diatom productivity (Marret et al., 2008).
191 Higher cyst concentrations are recorded between 850 and 450 cm (37.5 - 15.5 ka BP; mean
192 value of 3,000 cysts/cm^3), as well as between 90 and 30 cm (4 - 2.4 ka BP; mean value of
193 6,000 cysts/cm^3), for which two maxima are observed with 10,900 and 11,200 cysts/cm^3,
194 respectively (Figure 3). Increases in dinocyst concentrations are due to increasing occurrences
195 of *Operculodinium centrocarpum* or *Lingulodinium machaerophorum* (Figure 3).
196 Heterotrophic cyst concentrations (mainly led by *Brigantedinium* spp. and *Echinidinium*
197 species; Figure 3) as well as other cyst concentrations reach their maximal values during the
198 same main interval, i.e between 850 and 450 cm, but are three times lower for heterotrophics
199 (Figure 3). Higher abundance of heterotrophic cysts, mainly driven by *Brigantedinium* spp.
200 percentages all along the record (Figure 3), as well as those of *Echinidinium* spp. between 450
201 and 90 cm (15.5 - 4 ka BP; Figures 3 and 5), are strongly correlated with lower dinocyst
202 concentrations, especially between 15 and 4 ka BP (Figures 3 and 4). This could be consistent
203 with the fact that diatoms as well as dinoflagellates are the main food for strictly heterotrophic
204 dinoflagellates (Marret and Zonneveld, 2003), therefore echoing the previous idea of a
205 competition between dinoflagellate and diatom phytoplanktonic productivity in the study area
206 (Marret and Zonneveld, 2003).
207 Even if heterotrophic dinocyst concentrations can firstly be attributed to
208 dilution/concentration processes in sediments, the transition between generally higher cyst
209 concentrations and lower ones observed at 450 cm (15.5+/-0.4 ka BP) is synchronous with a
210 marked shift in biogenic opal ($BiSiO_2$) and total organic carbon (TOC) observed in a nearby
211 core (Schneider et al., 1997). This suggests different marine productivity patterns before and
212 after 15.5+/-0.4 ka BP. Based at least on the fact that these data indicate generally similar
213 trends, an atypical pattern is observed at 90 cm. While heterotrophic concentrations remain

low, and despite a relative stable trend characterized by still high terrigenous inputs (Bayon et al., 2012; Figure 3) as well as low $BiSiO_2$ and TOC values (Schneider et al., 1997), total dinocyst concentrations reach their maximum. To understand this atypical dinocyst concentration signal, indexes of specific diversity and dominance have been calculated to discuss periods possibly characterized by cyst advection (positive correlation between dominance and diversity) and *in situ* dinoflagellate productivity (negative correlation between dominance and diversity). Here, signals remain roughly anti-correlated all over the core, except at 90 cm (Figure 3), possibly due to a massive advection of *O. centrocarpum* at that time (Figure 3).

4.2 Dinocyst assemblages

Based on variations in cyst concentrations and in relative abundances of major species, five palynozones (A, B, C, D, E; Figure 3) have been visually established, then subdivided into several sub-palynozones (1, 2, 3; Figures 4 and 5) based on the rest of the assemblage (minor species always observed with at least >2%; Figures 4 and 5).

Temporal successions between dinocyst species can be observed all along the core,in particular for the dinocyst group mainly controlled by sea-surface salinity (Marret and Zonneveld, 2003), including *Spiniferites ramosus*, *Nematosphaeropsis labyrinthus*, *L. machaerophorum*, *O. centrocarpum* and *Operculodinium israelianum* (Figures 3, 4), as well as *Echinidinium* spp. (Figure 5). The first important succession occurred at 37.5 +/- 0.7 ka BP (limit between palynozones E and D), with a significant drop of the maximal relative abundances of *S. ramosus* and *N. labyrinthus*, then followed by maximal relative abundances of *L. machaerophorum* (Figure 4). At 32 +/- 0.7 ka BP (limit between palynozones D and C), a second major transition is related to a strong decline of *L. machaerophorum* synchronously with maximal percentages of *O. centrocarpum* , and then accompanied by *O. israelianum*

239 across the whole palynozone C (Figure 4). A third succession (limit between palynozone C
240 and B) is then observed between *O. centrocarpum* and *Echinidinium* spp. (Figures 4 and 5) at
241 15.5 +/- 0.4 ka BP, while the last major transition (limit B-A) evidences the important decline
242 of *Brigantedinium* spp. and strong re-increase of *O. centrocarpum* from 6 ka BP onwards,
243 together with the significant occurrence of *Spiniferites pachydermus* near the start of
244 palynozone A (a2, Figure 4).
245 Among the non-heterotrophics, the group of thermophile species comprises *Impagidinium*
246 *aculeatum, Impagidinium patulum, Spiniferites bentorii*, *Tuberculodinium vancampoae,*
247 *Spiniferites membranaceus* and *S. pachydermus*. This group also shows clear temporal
248 successions across the different palynozones (cf. Figure 4), in particular *S. pachydermus* at the
249 start of palynozone A (Figure 4). With regards to *Operculodinium aguinawense* (Figure 4), the
250 southernmost occurrences ever recorded of this species is observed in core KZAI-01. This
251 species only occurs today off the coasts of Cameroon and eastern Nigeria, in a small area
252 encompassing GeoB4905 core (Figure 6; Marret and Kim, 2009). Over the last 15.5 +/- 0.4
253 ka, variations of *O. aguinawense* percentages are relatively well correlated with the ones of
254 *Spiniferites mirabilis*, in particular across the Last Deglaciation. Today, both species are
255 restricted to the same area along the north equatorial African coast (Figure 6; Zonneveld et al.,
256 2013).
257 Among the heterotrophics, neritic taxa such as cysts of *P. schwartzii, Selenopemphix*
258 *nephroides*, and especially *Xandarodinium xanthum* as well as *Quinquecuspis concreta*
259 (Figure 5), show extremely close occurrences all along the core. This is especially obvious
260 between 37 +/- 0.7 and 7 +/- 0.2 ka BP (Figure 5), and maximal percentages of these species
261 are recorded around 36 - 32, 25 - 20 and 15.5 - 7 ka BP (Figure 5). Also, another important
262 feature is the disappearance of cysts of *P. schwartzii* around 35 +/- 0.4 ka BP, synchronously
263 with a significant increase of *S. nephroides* at that time (Figure 5; limit between sub-

264 palynozones d2 and d1).

265

266 **5. DISCUSSION**

267 ***5.1. Orbital control on past dinoflagellate productivity regimes***

268 *5.1.1. Dinoflagellate productivity on the Congolese margin: Congo River versus upwelling*
269 *dynamics*

270 Over the last glacial cycle, it is commonly accepted (Dupont et al., 1998; Shi et al., 1998;
271 Dupont and Behling, 2006; Kim et al., 2010; Zonneveld et al., 2013) that in the intertropical
272 band higher primary productivity occurred during periods of global cooling such as the LGM
273 or Greenland Stadials (GS, including Heinrich Stadials or HS), in response to intensified
274 upwelling cells. Inversely, during warmer and wetter periods such as Greenland Interstadials
275 (GI) or the Holocene, characterized by higher riverine inputs, primary productivity is low.
276 Within our dinocyst record, higher dinoflagellate productivity seems to be recorded during the
277 last glacial until 15.5 +/- 0.4 ka BP (high cyst concentrations), consistently with high values
278 of $BiSiO_2$ and TOC observed in the neighbour core GeoB 1008 (Schneider et al., 1997; Figure
279 3). Furthermore, *Trinovantedinium applanatum*, a typical well-known coastal upwelling
280 species (Marret and Zonneveld, 2003), mainly occurred between 28 +/- 0.6 and 19 +/- 0.3 ka
281 BP (palynozones c3 to c2; Figures 5 and 7), consistently with the idea of stronger upwelling
282 cells across glacial maxima, and more specifically here during MIS 2, in a dry context
283 characterized by weak terrigenous supplies to the Congo margin, and cold sea-surface
284 conditions (Figures 4 and 6).
285 At the onset of the Last Deglaciation, around 15.5 +/- 0.4 ka BP, a quasi-disappearance of the
286 *T. applanatum* signal is observed (Figures 5 and 7). However, heterotrophic percentages
287 remain high and are even characterized, between 15.5 +/- 0.4 and 7 +/- 0.2 ka BP (sub-
288 palynozones b2 and b3), by the highest values ever recorded (Figures 5 and 7). This leads us

289 to consider, at that time, another major source of nutrients to the ocean than upwelling cells.
290 The relatively good consistency between major element terrestrial signals (cf. XRF ratios in
291 KZAI-01 core), percentages of heterotrophic (*Brigantedinium* spp.) as well as fluvial-
292 sensitive cysts (*Echinidinium* spp., river-plume taxa) (Figures 5 and 7), suggests that nutrient-
293 rich freshwater discharges from the Congo River probably acted as a major driving factor for
294 promoting dinoflagellate productivity in the study area, especially across the Last
295 Deglaciation, but also during MIS 3. Furthermore, between 15.5 +/- 0.4 and 7 +/- 0.2 ka BP,
296 continental shelf reworking, induced by the post-glacial sea-level rise, may have also
297 represented an additional source of nutrients to the ocean (Marret et al., 2008), also
298 contributing to slightly enhanced dinoflagellate productivity at that time (Figures 5 and 7).
299
300 *5.1.2 Precession versus Obliquity accounting for different fluvial regimes*
301 The influence of orbital forcing on low latitude atmospheric processes is still a matter of
302 debate. The tropical response to obliquity forcing appears to be the remote influence of high-
303 latitude glacial ice-sheet oscillations (deMenocal et al., 1993), in parallel with significant
304 changes in cross-equatorial insolation gradient (Bosmans et al., 2015). Precession forcing is
305 more important in low latitude moisture changes, i.e warmer and wetter conditions in the
306 hemisphere where summer solstice occurred at the Earth perihelion (Merlis et al., 2012).
307 Furthermore, it has been inferred that the precession / obliquity combination has also a great
308 influence on monsoon oscillations with a significant prevalence of the precession forcing
309 (Tuenter et al., 2003). More precisely, minima of precession would correspond to an
310 intensification of the monsoonal activity, and obliquity would tend to mitigate (minima of
311 obliquity) or enhance (maxima of obliquity) the initial precession forcing (Tuenter et al.,
312 2003). The orbital variations have therefore changed significantly the latitudinal spread of
313 precipitations in consequence of oceanic heat gradient variations (Stager et al., 2011; McGee

et al., 2014).

In our dinocyst record, significant occurrences of fluvial-sensitive cysts (especially *L. machaerophorum* and *Echinidinium* spp.) appear to correspond to minima of precession, thus suggesting wetter conditions in the study area (Figure 7). This is especially observed during the Last Deglaciation - early Holocene between 15.5 +/- 0.4 and 4 +/- 0.15 ka BP (with the prevalence of *Echinidinium* spp.), as well as during the MIS 3 interval between 39 +/-0.9 and 32 +/-0.7 ka BP (with the prevalence of *L. machaerophorum*). Superimposed on this general pattern, a combination "minimum of precession - maximum of obliquity" would explain the optimal orbital combination for high moisture conditions according to Tuenter et al. (2003). This configuration indeed occurred between 16 and 6 ka BP in our dinocyst results and corresponds to the maximal recorded values of fluvial-sensitive cysts (*Echinidinium* spp.) in combination with the highest values of heterotrophic cyst percentages (mainly including *Brigantedinium* spp.) (Figure 7).

The minimum of precession recorded during MIS 3 (Figure 7) is characterized by a decreasing trend of Earth's obliquity, and is also consistently characterized by a weaker Ti/Ca ratio and associated lower surface productivities between 39 +/- 0.9 and 32 +/- 0.7 ka BP (Figure 7). Despite the austral location of KZAI-01 core, dinocyst assemblages indicate wetter conditions during precession minima (Figure 7), i.e when Earth perihelion occurred during northern summer solstice, with associated drier conditions in the Southern Hemisphere (Merlis et al., 2012). Conversely, maxima of precession, supposed to be favourable for wetter conditions in the Southern Hemisphere, correspond to periods with lower terrigenous inputs, especially between 44 +/- 1.6 and 39 +/- 0.9 ka BP (subpalynnozone e2) and between 25 +/- 0.5 and 16 +/- 0.2 ka BP (subpalynozones c2 and c1; Figure 7).

339 *5.1.3. The atypical signature of MIS 2*

340 In the tropics, during MIS 2, the latitudinal contraction of the TR resulted in colder conditions
341 on the continent (Powers et al., 2005; Tierney et al., 2011; Loomis et al., 2012) with the
342 establishment of open landscape (Anhuf et al., 2006), and cold surface waters (deMenocal et
343 al., 2000; Weldeab et al., 2005; Shakun and Carlson, 2010). This widely observed pattern is in
344 agreement with the low terrigenous signal recorded on core KZAI-01 (Figure 7) that suggests
345 reduced weathering conditions combined with lower terrestrial erosion at that time. Paleo-
346 precipitation reconstructions (Bonnefille and Chalié, 2000) also suggest generally low values
347 in the Congo Basin, however characterized by a complex pattern oscillating between slightly
348 wetter and drier conditions. In our dinocyst record, low occurrences of *T. applanatum*,
349 *Selenopemphix quanta* (Figure 5) and cysts of *Pentapharsodinium dalei* (Appendix) are
350 consistent with the tropical glacial period, mainly influenced by upwelling dynamics under
351 dry climate.

352 However, between 25 +/- 0.5 and 17 +/- 0.25 ka BP (sub-palynozones c2 and c3; Figure 7),
353 low relative abundances of *Echinidinium* spp. as well as high percentages of *L.*
354 *machaerophorum* (up to 50 %) would suggest strengthened river discharges and thus wetter
355 conditions consistent with the general pattern of Austral moisture during maximal values of
356 the precession index. Even if an influence of lower sea level on the neritic ecology of both
357 *Echinidinium* spp. and *L. Machaerophorum* during this time cannot be ruled out entirely, this
358 pattern can possibly be explained by the cross-equatorial location of the Congo Basin
359 therefore benefiting from Southern Hemisphere wetter configurations, the Northern Congo
360 Basin corresponding to a third of the whole surface. However, northern tributary rivers
361 contribute half the total discharge (Bultot, 1971; Lempicka, 1971) and it is important to note
362 the general greater influence of northern rivers in comparison with austral ones within the
363 Congo Basin. Terrigenous inputs to the ocean will then remain more important when the

364 northern basin will be fed by strengthened precipitations in a boreal context of precession
365 minima.
366 Another atypical dinocyst signature of MIS 2 is based on the occurrence of thermophile
367 species (*S. mirabilis*, *S. membranaceus*, *S. bentorii* and *T. vancampoae*), currently found in
368 equatorial warm waters (Figure 6), which mainly occurred between 21 +/- 0.4 and 17 +/- 0.25
369 ka BP, after a gradual increase noted from the beginning of the LGM (Figures 4 and 5). The
370 southward shift of the TR and the equatorial warm waters until 2°S (Arbuszewsky et al.,
371 2013) may have brought heat and moisture to the study area while other parts of the
372 Equatorial Atlantic remained colder and drier (Stager et al., 2011). Furthermore, the world
373 atlas of modern dinocysts (Zonneveld et al., 2013) also describes these thermophile species as
374 being oligotrophic to mesotrophic. Their occurrences during MIS 2 could thus suggest such
375 conditions in the study area, consistently with recorded lower terrigenous inputs during this
376 period (Figures 3 and 7), while high percentages of heterotrophic taxa (up to 40 % of dinocyst
377 assemblages during MIS 2, especially coastal warm heterotrophic taxa) would rather evidence
378 mesotrophic conditions during this interval, consistent with present-day trophic conditions
379 characterizing coastal equatorial waters.
380
381 *5.1.4 Eastern and Western African monsoons: complex interferences in the Congo Basin*
382 The large area of the Congo Basin raises the question of the complex interferences between
383 Western and Eastern African monsoon systems. The atmosphere above the catchment area is
384 indeed divided by the Congo Air Boundary (CAB) convergence zone (Tierney et al., 2011),
385 delineating the border between the western and eastern African monsoons. Past oscillations of
386 these different monsoon clusters have been simulated (Caley et al., 2011; Figure 7) from
387 paleo-river discharges of the Niger (Western African monsoon) and of the Nile (Eastern
388 African monsoon), and have also been reconstructed through Ba/Ca ratios of *Globigerinoides*

389 *ruber* (MD32-2707 core; Figures 1 and 7; Weldeab et al., 2007). As mentioned above,
390 dinocyst river-plume assemblages of KZAI-01 core strongly develop in response to boreal
391 summer river discharges linked with precession minima (Figure 7), suggesting that the
392 Western African monsoon can be considered as the main forcing for northern summer
393 rainfalls in the Congo Basin. This common pattern is particularly well highlighted during the
394 Last Deglaciation, when relative abundances of river-plume taxa increase in parallel with
395 terrigenous signals shortly after the increase of the Western African monsoon, around 16 +/-
396 0.2 ka BP (Figure 7). Furthermore, the maximum of the West African monsoon activity
397 between 8 and 6 ka BP (Figure 7) also corresponds with the highest occurrences of *O.*
398 *aguinawense*, evidencing a great relationship between the Western African monsoonal forcing
399 and the establishment of near equatorial conditions during this period (cf. Figure 6; Marret
400 and Kim, 2009).
401 However, the relationship described above between Western African monsoon signal and
402 dinocyst assemblages is less clear during the recorded wetter interval ranging from 39 +/- 0.9
403 to 27.5 +/- 0.7 ka BP (Figure 7). Our dinocyst data would indeed suggest a better correlation
404 with the maximum of the Eastern African monsoon signal (Figure 7) while the Western one
405 remained weakened. This pattern is well correlated with estimates of paleoprecipitation
406 inferred from pollen extracted from Burundi mounts (Bonnefille and Chalié, 2000), which
407 display higher precipitations during this interval, also in accordance with strengthened Eastern
408 African monsoons (Figure 7).
409
410 ***5.2. Sub-orbital variations over the last 20 ky***
411 *5.2.1. The Last Deglaciation*
412 *The tropical response of Heinrich Stadial 1 (HS1)*
413 Between 18 +/- 0.3 and 15.5 +/- 0.4 ka BP, relative abundances of thermophile and river-

plume species dropped sharply while *O. centrocarpum* reached very high percentages (up to 50%) at that time (sub-palynozone c1; Figure 8). Present-day distribution of *O. centrocarpum* in the South Atlantic Ocean shows a strong relationship with northward cold currents (including the BC) (Figure 6; Zonneveld et al., 2013), especially during the austral winter when cold currents reach the equatorial area. High percentages of *O. centrocarpum* may thus suggest a greater influence of the BC advection in our study area between 18 and 15.5 ka BP. The increase in *O. centrocarpum* percentages is also noticeable within the Benguela Upwelling system (GeoB1023 core; Figures 1 and 8; Shi et al., 1998), also highlighting the BC activity at a larger regional-scale. Combined with occurrences of *T. applanatum* at that time (Figure 8), which today is typical of the modern Benguela Upwelling System along the Angolan margin (Holzwarth et al., 2000; Zonneveld et al., 2013), both species would thus indicate a cold and dry climate, consistent with previous studies that described a strong drought on the African continent (Stager et al., 2002, 2011; Bouimetarhan et al., 2012; Weldeab, 2012). More precisely, low precipitation (Bonnefille and Chalié, 2000; Schefuß et al., 2005; Figure 7) were recorded as well as a continental and marine cooling ranging between 1 and 2°C below mean LGM values (Müller et al., 1998; Powers et al., 2005; Weldeab et al., 2005; Weldeab et al., 2007; Loomis et al., 2012).

This cool and dry event appears synchronous with a massive advection of freshwater that occurred in the North Atlantic during Heinrich Stadial (HS) 1. The tropical response of HS 1 would then consist of a southward shift of the TR (Arbuszewski et al., 2013; McGee et al., 2014), involving a contraction of the latitudinal belts (Stager et al., 2011) and weakened monsoons during this period. It is interesting to note that while dinocysts suggest a marked sea-surface cooling, isotopic signals from nearby core GeoB6518-1 (Schefuß et al., 2005; Figure 8) suggest a steady increase in tropical moisture during HS1. This implies a fundamental divergence between marine and continental compartments across the Last

439 Deglaciation.

440

441 *The equatorial signal of increasing deglacial warming at 15.5 ka BP*

442 Around 15.5 - 15 ka BP, the equatorial deglacial transition occurred in parallel with a global
443 warming (Weldeab et al., 2005; Weijers et al., 2007; Leduc et al., 2010), linked with the
444 Northern Hemisphere July insolation increase. This resulted in a northward shift of the TR
445 (Arbuszewski et al., 2013; McGee et al., 2014) and thus strengthened monsoon.
446 Our dinocyst data also show a significant increase in percentages of *Brigantedinium* spp. and
447 *Echinidinium* spp. at around 15.5 +/- 0.4 ka BP (limit between palynozones B and C; Figure
448 8). Their modern distributions in the tropics are related of both nutrient-enriched waters and,
449 more specifically for *Echinidinium* spp., to high river-discharges (Zonneveld et al., 2013).
450 This is consistent with the strong increase of terrigenous inputs observed at that time in the
451 same core (Bayon et al., 2012; Figure 8). The equatorial species *O. aguinawense* also
452 appeared shortly at around 15.5 ka BP (Figure 8), suggesting near equatorial conditions
453 during this short event. Relative abundances of *L. machaerophorum* also increased again at
454 15.5 ka BP but remained low in comparison with glacial ones, suggesting a specific switch in
455 fluvial-sensitive dinocyst tracers between *L. machaerophorum* (glacial) and *Echinidinium* spp.
456 (across and after the Last Deglaciation).
457 Among the thermophile species, *Selenopemphix nephroides* and especially *Stelladinium reidii*
458 are the clearest signals of the post 15.5 ka BP deglacial warming (Figure 8). Both species are
459 also considered good tracers for regimes of high trophic conditions (Zonneveld et al., 2013),
460 in agreement with the recorded surface nutrient enrichment previously suggested during this
461 period (cf. *Brigantedinium* spp. and *Echinidinium* spp.). Extremely low abundances of *O.*
462 *centrocarpum* at that time could be interpreted as minor or non-existent influence of the BC in
463 the study area (Figure 8), while significant abundances of this species recorded in GeoB1023

core (cf. Figure 1; Shi et al., 1998) would conversely suggest a strengthening of this cold current. This may be the consequence of a 3° southward latitudinal shift of the ABF between 15 and 7 ka BP(Figure 8), disconnecting the study area from the influence of the Benguela Upwelling system.

The tropical response of the Younger Dryas (YD)

Significant dinocyst changes occurred between around 13 +/- 0.2 and 11.5 +/- 0.35 ka BP in both dinocyst and geochemical records (Figure 8). The significant drop of XRF Ti/Ca ratio evidences a reduction of terrigenous input, while percentages of thermophile species *S. mirabilis*, *S. nephroides* and *S. reidii* strongly decrease, suggesting a significant cooling of surface waters in the study area. The recorded cooling would be in agreement with the Younger Dryas timing (Lowe and Hoek, 2001) (Figure 8). However, high abundances of *Echinidinium* spp. and *Brigantedinium* spp. during this interval suggest that nutrient-enriched river discharges still occurred at that time (Figure 8). Wetter conditions could be explained by a suitable location of the TR above the Congo Basin, between Holocene and LGM mean locations (Arbuszewski et al., 2013; McGee et al., 2014). Furthermore, the weakening of the deglacial sea-level rise during this period (Grant et al., 2012) and therefore the decrease of associated continental shelf reworking (Marret et al., 2008) could explain the observed drop in terrigenous inputs and the long-term decreasing trend of *Echinidinium* spp. (Figure 8). The absence of *T. applanatum* during the tropical response of the YD would also suggest the absence of upwelling cells in the study area (Figure 7). Nevertheless, high abundance of *S. quanta* and *S. membranaceus* (Figures 5 and 8), generally abundant in the vicinity of seasonal upwelling cells (Marret and Zonneveld, 2003), may suggest the development of seasonal coastal upwelling close to the study area.

489 *5.2.2 The Holocene*

490 Aknowledging the weak chrono-stratigraphic constraint of the Holocene (cf. Figure 2), some
491 major subdivisions of the Holocene (Early-, Mid-, and Late-Holocene) can be discussed
492 nevertheless.

493

494 *The Early Holocene and the African Humid Period*

495 Across the Holocene, the African Humid Period (AHP) is a significantly warmer and wetter
496 period that occurred between around 14.5 and 5 ka BP (deMenocal et al., 2000; Shanahan et
497 al., 2015). At that time, the TR was characterized by a wider latitudinal extension up to
498 several degrees poleward (Stager et al., 2011; Arbuszewski et al., 2013; McGee et al., 2014).
499 Previous dinocyst studies showed that the AHP was characterized by the gradual bloom of
500 thermophile (*S. mirabilis*) and low-salinity (*O. aguinawense*) species, induced by
501 strengthened river discharges from the beginning of the Holocene (Dupont and Behling, 2006;
502 Kim et al., 2010; Marret et al., 2013).
503 Similar to these studies, our record also evidences a strengthening of nutrient-enriched river
504 discharges from the onset of the Last Deglaciation (Figure 8; cf. subchapter 5.2.1). However
505 significant occurrences of *O. aguinawense* between around 11 +/- 0.35 and 2 +/- 0.2 ka BP
506 (Figure 8) delimit the effective wettest period, also characterized by the highest abundances of
507 both mesotrophic and eutrophic thermophile species (Figure 8). High SST recorded at the
508 beginning of the Holocene are also well correlated with alkenone SST reconstructions from
509 core GeoB6518 (Schefuß et al., 2005) synchronously with the Early Holocene timing (Figure
510 8). It is interesting to note that, during this Holocene climatic optimum, our dinocyst data
511 show a sharp drop of *Echinidinium* spp. relative abundances between 8 and 7 ka BP,
512 synchronously with a drop of thermophile species (Figure 8). This could suggest a thousand
513 years-long cooler and drier event that occurred during the Early and Mid-Holocene transition

514 (Walker et al., 2012).

515

516 *The Mid-Holocene transition and the end of the African Humid Period*

517 The timing of the AHP termination varies significantly between studies, i.e around 2.5 ka BP
518 (Kröpelin et al., 2008; Lézine et al., 2013; Shanahan et al., 2012; Lebamba et al., 2012), 4 ka
519 BP (deMenocal et al., 2000; Hély et al., 2009; Tierney and deMenocal, 2013; Shanahan et al.,
520 2015), or even earlier at around 5.3 ka BP (Lézine et al., 2005). Consequently, the duration of
521 the AHP also varies between these, from a few centuries to a few thousand years according to
522 the references mentioned above (Figure 8).
523 In our data, we observe two events characterised by abrupt cooling and drying conditions. The
524 first decline occurred abruptly between 7 +/- 0.15 and 6 +/- 0.1 ka BP (transition between sub-
525 palynozones b1 and b2), illustrated by the sharp drop of heterotrophic taxa percentages,
526 especially *Brigantedinium* spp., *S. reidii* and *S. nephroides* (Figure 8), in parallel with high
527 relative abundances of *O. centrocarpum*. This suggests an environmental change from
528 eutrophic to less nutrient-rich surface waters, probably allowing the observed development of
529 mesotrophic taxa, such as *S. mirabilis* (Figure 8). This decrease does not appear as a dry
530 event, due to: i) the persistence of high *Echinidinium* spp. percentages, with however a long-
531 term decreasing trend obvious since 15.5 +/- 0.4 ka BP (Figure 8), and ii) the persistence of *O.*
532 *aguinawense* (today related to near-equatorial hydrological conditions; cf. Figure 6) which
533 reached its highest relative abundances during this interval (sub-palynozone b1, Figure 8).
534 The second decrease occurred abruptly between 4 +/- 0.08 and 3.5 +/- 0.08 ka BP (transition
535 between palynozones A and B; Figure 8), as displayed by a general drop of both heterotrophic
536 and thermophile cyst percentages, while *O. centrocarpum* rapidly became the major dinocyst
537 species (Figure 8). As we discussed above from crossed information related to total dinocyst
538 concentrations and community indexes (dominance *versus* diversity; cf. Section 4.1 and

539 Figure 3), the interval ranging from 4 +/- 0.08 to 2.5 +/- 0.08 ka BP (sub-palynozone a2;
540 Figure 8) is probably characterized by massive advection of *O. centrocarpum* cysts. However,
541 removing *O. centrocarpum* percentages from the abundance calculations of other taxa will not
542 erase the observed shift discussed above for heterotrophic and thermophile dinocysts, clearly
543 related to the 4 - 3.5 ka BP period.
544
545 *The Late Holocene*
546 Right after 3.5 +/- 0.08 ka BP the interval appears to be one of the coolest and driest periods
547 recorded in core KZAI-01, as evidenced by the strong dominance of *O. centrocarpum*, and as
548 also previously observed in GeoB1023 core (Figure 8; Shi et al., 1998). This could be the
549 consequence of a strengthened BC activity, maybe also related to a 4° northward shift of the
550 ABF, well recorded during the Mid- to Late Holocene (Figure 8, Jansen et al., 1996).
551 Finally, from 2.5 +/- 0.08 ka BP onward (subpalynozone a1), a recovery of *L.*
552 *machaerophorum* and *Echinidinium* spp. percentages is observed in parallel with low
553 occurrences of *O. aguinawense* (Figures 5 and 8), suggesting a slight re-increase of wetter
554 conditions. However, despite the general tropical warming observed in several SST
555 reconstructions over this period (Schefuß et al., 2005; Weldeab et al., 2005; Dyez et al., 2014),
556 all thermophile cyst percentages remain null or very low (Figure 8). The recovery of wetter
557 conditions may be explained by the optimum of the precession index around 3 ka BP (Figure
558 7), which implies the correspondence between austral summer and Earth perihelion and
559 allows the establishment of wetter and warmer conditions in the Southern Hemisphere.
560 The Holocene, as recorded in core KZAI-01, thus can be divided into three major periods.
561 The earliest interval (11 +/- 0.35 - 6.5 +/- 0.1 ka BP) is also the warmest and wettest period,
562 followed, between 6.5 +/- 0.1 and 4 +/- 0.08 ka BP, by a less warm and humid period,
563 characterized by the progressive recovery of the BC activity. Finally, after 4 ka BP, a major

long-term cooling and drying period is gradually pondered by a progressive recovery of river discharges in the study area since 2.5 ka BP.

6. CONCLUSION

Analysis of dinocyst assemblages in core KZAI-01 has permitted an investigation of land-sea-atmosphere linkages off the Congo River mouth over the last 44 ky. Our dinocyst data evidence a great influence of nutrient-rich river discharges caused by latitudinal migrations of the tropical tainbelt, forced by different orbital configurations, and especially regarding the combination "precession minima - obliquity maxima". Furthermore, while most of studies describe the LGM as a "cold and dry" period in the tropics, thermophile and river-plume dinocysts evidence here a pattern relatively similar to modern warm equatorial assemblages. The LGM appears to be a complex period characterized by a southward shift of the monsoonal belt and of warm surface waters, bringing heat and moisture. This illustrates a complex dynamics that warrant model simulations to explore the underlying mechanisms that occurred across this specific climate interval.

This high-resolution study has also permitted to discriminate major climate periods of the Last Deglaciation in good correspondence with Northern Hemisphere high latitude millennial-scale oscillations. We also discuss the timing of the equatorial response of the African Humid Period and the two-steps decrease in heat and moisture conditions in the study area. Further work will involve a regional-scale study including other dinocyst records to reconstruct sea-surface environments in relationship with latitudinal shifts in the tropical rainbelt along the Western African coast, as well as model-data inter-comparisons for different snapshots across the last glacial, deglacial and Holocene periods.

7. ACKNOWLEDGEMENTS

W. Hardy's PhD was funded by Brittany Region and this work was supported by the "Laboratoire d'Excellence" LabexMER (ANR-10-LABX-19) and co-funded by a grant from the French government under the program "Investissements d'Avenir". We thank Mr. B. Dennielou (Ifremer, Brest) for access to core KZAI-01. We thank the two anonymous reviewers for their constructive comments that helped to improve this manuscript.

8. REFERENCES

Anhuf, D., Ledru, M.-P., Behling, H., Da Cruz Jr., F. W., Cordeiro, R. C., Van der Hammen, T., Karmann, I., Marengo, J. A., De Oliveira, P. E., Pessenda, L., Siffedine, A., Albuquerque, A. L. and Da Silva Dias, P. L.: Paleo-environmental change in Amazonian and African rainforest during the LGM, Palaeogeography, Palaeoclimatology, Palaeoecology, 239(3–4), 510–527, doi:10.1016/j.palaeo.2006.01.017, 2006.

Anka, Z., Séranne, M., Lopez, M., Scheck-Wenderoth, M. and Savoye, B.: The long-term evolution of the Congo deep-sea fan: A basin-wide view of the interaction between a giant submarine fan and a mature passive margin (ZaiAngo project), Tectonophysics, 470(1–2), 42–56, doi:10.1016/j.tecto.2008.04.009, 2009.

Antoine, D., André, J.-M. and Morel, A.: Oceanic primary production: 2. Estimation at global scale from satellite (Coastal Zone Color Scanner) chlorophyll, Global Biogeochem. Cycles, 10(1), 57–69, doi:10.1029/95GB02832, 1996.

Arbuszewski, J. A., deMenocal, P. B., Cléroux, C., Bradtmiller, L. and Mix, A.: Meridional shifts of the Atlantic intertropical convergence zone since the Last Glacial Maximum, Nature Geosci, 6(11), 959–962, doi:10.1038/ngeo1961, 2013.

Babonneau, N., Savoye, B., Cremer, M. and Klein, B.: Morphology and architecture of the present canyon and channel system of the Zaire deep-sea fan, Marine and Petroleum Geology, 19(4), 445–467, doi:10.1016/S0264-8172(02)00009-0, 2002.

Bayon, G., Dennielou, B., Etoubleau, J., Ponzevera, E., Toucanne, S. and Bermell, S.: Intensifying Weathering and Land Use in Iron Age Central Africa, Science, 335(6073), 1219–1222, doi:10.1126/science.1215400, 2012.

Berger, A. and Loutre, M. F.: Insolation values for the climate of the last 10 million years, Quaternary Science Reviews, 10(4), 297–317, doi:10.1016/0277-3791(91)90033-Q, 1991.

Bonnefille, R. and Chalié, F.: Pollen-inferred precipitation time-series from equatorial mountains, Africa, the last 40 kyr BP, Global and Planetary Change, 26(1–3), 25–50, doi:10.1016/S0921-8181(00)00032-1, 2000.

Bosmans, J. H. C., Hilgen, F. J., Tuenter, E. and Lourens, L. J.: Obliquity forcing of low-latitude climate, Clim. Past, 11(10), 1335–1346, doi:10.5194/cp-11-1335-2015, 2015.

Bouimetarhan, I., Prange, M., Schefuß, E., Dupont, L., Lippold, J., Mulitza, S. and Zonneveld, K.: Sahel megadrought during Heinrich Stadial 1: evidence for a three-phase evolution of the low- and mid-level West African wind system, Quaternary Science Reviews, 58, 66–76, doi:10.1016/j.quascirev.2012.10.015, 2012.

Bultot, F.: Atlas climatique du bassin congolais, I.N.É.A.C., 1971.

Caley, T., Malaizé, B., Revel, M., Ducassou, E., Wainer, K., Ibrahim, M., Shoeaib, D., Migeon, S. and Marieu, V.: Orbital timing of the Indian, East Asian and African boreal monsoons and the concept of a “global monsoon,” Quaternary Science Reviews, 30(25–26), 3705–3715, doi:10.1016/j.quascirev.2011.09.015, 2011.

Collier, A. B. and Hughes, A. R. W.: Lightning and the African ITCZ, Journal of Atmospheric

635 and Solar-Terrestrial Physics, 73(16), 2392–2398, doi:10.1016/j.jastp.2011.08.010, 2011.

636 da Cunha, L. C. and Buitenhuis, E. T.: Riverine influence on the tropical Atlantic Ocean
637 biogeochemistry, Biogeosciences, 10(10), 6357–6373, doi:10.5194/bg-10-6357-2013, 2013.

638 deMenocal, P., Ortiz, J., Guilderson, T., Adkins, J., Sarnthein, M., Baker, L. and Yarusinsky,
639 M.: Abrupt onset and termination of the African Humid Period:: rapid climate responses to
640 gradual insolation forcing, Quaternary Science Reviews, 19(1–5), 347–361,
641 doi:10.1016/S0277-3791(99)00081-5, 2000.

642 deMenocal, P. B., Ruddiman, W. F. and Pokras, E. M.: Influences of High- and Low-Latitude
643 Processes on African Terrestrial Climate: Pleistocene Eolian Records from Equatorial Atlantic
644 Ocean Drilling Program Site 663, Paleoceanography, 8(2), 209–242, doi:10.1029/93PA02688,
645 1993.

646 Droz, L., Marsset, T., Ondréas, H., Lopez, M., Savoye, B. and Spy-Anderson, F.-L.:
647 Architecture of an active mud-rich turbidite system: The Zaire Fan (Congo–Angola margin
648 southeast Atlantic) Results from ZaïAngo 1 and 2 cruises, AAPG Bulletin, 87(7), 1145–1168,
649 doi:10.1306/03070300013, 2003.

650 Dupont, L. and Behling, H.: Land–sea linkages during deglaciation: High-resolution records
651 from the eastern Atlantic off the coast of Namibia and Angola (ODP site 1078), Quaternary
652 International, 148(1), 19–28, doi:10.1016/j.quaint.2005.11.004, 2006.

653 Dupont, L. M., Marret, F. and Winn, K.: Land-sea correlation by means of terrestrial and
654 marine palynomorphs from the equatorial East Atlantic: phasing of SE trade winds and the
655 oceanic productivity, Palaeogeography, Palaeoclimatology, Palaeoecology, 142(1–2), 51–84,
656 doi:10.1016/S0031-0182(97)00146-6, 1998.

657 Dyez, K. A., Zahn, R. and Hall, I. R.: Multicentennial Agulhas leakage variability and links to
658 North Atlantic climate during the past 80,000 years, Paleoceanography, 29(12),
659 2014PA002698, doi:10.1002/2014PA002698, 2014.

660 F Fatela, R. Taborda.: Confidence limits of species proportions in microfossil assemblages,
661 Marine Micropaleontology, 45(2), 169–174, doi:10.1016/S0377-8398(02)00021-X, 2002.

662 Gordon, A. L., Bosley, K. T. and Aikman III, F.: Tropical atlantic water within the Benguela
663 upwelling system at 27°S, Deep Sea Research Part I: Oceanographic Research Papers, 42(1),
664 1–12, doi:10.1016/0967-0637(94)00032-N, 1995.

665 Hansen, M. C., Potapov, P. V., Moore, R., Hancher, M., Turubanova, S. A., Tyukavina, A.,
666 Thau, D., Stehman, S. V., Goetz, S. J., Loveland, T. R., Kommareddy, A., Egorov, A., Chini,
667 L., Justice, C. O. and Townshend, J. R. G.: High-Resolution Global Maps of 21st-Century
668 Forest Cover Change, Science, 342(6160), 850–853, doi:10.1126/science.1244693, 2013.

669 Heezen, B. C. and Hollister, C.: Deep-sea current evidence from abyssal sediments, Marine
670 Geology, 1(2), 141–174, doi:10.1016/0025-3227(64)90012-X, 1964.

671 Hély, C., Braconnot, P., Watrin, J. and Zheng, W.: Climate and vegetation: Simulating the
672 African humid period, Comptes Rendus Geoscience, 341(8–9), 671–688,
673 doi:10.1016/j.crte.2009.07.002, 2009.

674 Hirahara, S., Ishii, M. and Fukuda, Y.: Centennial-Scale Sea Surface Temperature Analysis
675 and Its Uncertainty, J. Climate, 27(1), 57–75, doi:10.1175/JCLI-D-12-00837.1, 2013.

676 Holzwarth, U., Esper, O. and Zonneveld, K.: Distribution of organic-walled dinoflagellate
677 cysts in shelf surface sediments of the Benguela upwelling system in relationship to
678 environmental conditions, Marine Micropaleontology, 64(1–2), 91–119,
679 doi:10.1016/j.marmicro.2007.04.001, 2007.

680 Hsu, C.-P. F. and Wallace, J. M.: The Global Distribution of the Annual and Semiannual
681 Cycles in Precipitation, Mon. Wea. Rev., 104(9), 1093–1101, doi:10.1175/1520-
682 0493(1976)104<1093:TGDOTA>2.0.CO;2, 1976.

683 Jansen, J. H. F., Ufkes, E. and Schneider, R. R.: Late Quaternary Movements of the Angola-
684 Benguela Front, SE Atlantic, and Implications for Advection in the Equatorial Ocean, in The
685 South Atlantic, pp. 553–575, Springer Berlin Heidelberg. [online] Available from:
686 http://scdproxy.univ-brest.fr:2068/chapter/10.1007/978-3-642-80353-6_28 (Accessed 28
687 October 2014), 1996.

688 John Lowe, J. and Hoek, W. Z.: Inter-regional correlation of palaeoclimatic records for the
689 Last Glacial–Interglacial Transition: a protocol for improved precision recommended by the
690 INTIMATE project group, Quaternary Science Reviews, 20(11), 1175–1187,
691 doi:10.1016/S0277-3791(00)00183-9, 2001.

692 Khripounoff, A., Vangriesheim, A., Babonneau, N., Crassous, P., Dennielou, B. and Savoye,
693 B.: Direct observation of intense turbidity current activity in the Zaire submarine valley at
694 4000 m water depth, Marine Geology, 194(3–4), 151–158, doi:10.1016/S0025-
695 3227(02)00677-1, 2003.

696 Kim, S.-Y., Scourse, J., Marret, F. and Lim, D.-I.: A 26,000-year integrated record of marine
697 and terrestrial environmental change off Gabon, west equatorial Africa, Palaeogeography,
698 Palaeoclimatology, Palaeoecology, 297(2), 428–438, doi:10.1016/j.palaeo.2010.08.026, 2010.

699 Kröpelin, S., Verschuren, D., Lézine, A.-M., Eggermont, H., Cocquyt, C., Francus, P., Cazet,
700 J.-P., Fagot, M., Rumes, B., Russell, J. M., Darius, F., Conley, D. J., Schuster, M.,
701 Suchodoletz, H. von and Engstrom, D. R.: Climate-Driven Ecosystem Succession in the
702 Sahara: The Past 6000 Years, Science, 320(5877), 765–768, doi:10.1126/science.1154913,
703 2008.

704 Lass, H. U. and Mohrholz, V.: On the interaction between the subtropical gyre and the
705 Subtropical Cell on the shelf of the SE Atlantic, Journal of Marine Systems, 74(1–2), 1–43,
706 doi:10.1016/j.jmarsys.2007.09.008, 2008.

707 Lebamba, J., Vincens, A. and Maley, J.: Pollen, vegetation change and climate at Lake
708 Barombi Mbo (Cameroon) during the last ca. 33 000 cal yr BP : a numerical approach,
709 Climate of the Past, 8(1), 59–78, doi:10.5194/cp-8-59-2012, 2012.

710 Leduc, G., Schneider, R., Kim, J.-H. and Lohmann, G.: Holocene and Eemian sea surface
711 temperature trends as revealed by alkenone and Mg/Ca paleothermometry, Quaternary
712 Science Reviews, 29(7–8), 989–1004, doi:10.1016/j.quascirev.2010.01.004, 2010.

713 Lempicka, M.: Lempicka (Magdalena), Bilan hydrique du bassin du fleuve Zaïre. 1ère Partie :
714 Ecoulement du bassin 1950-1959. Kinshasa : Office National de la Recherche et du

715 Développement (ONRD), 1971, 147 p., Office National de la Recherche et du Développement
716 (ONRD), Kinshasa., 1971.

717 Leroux, M.: The Meteorology and Climate of Tropical Africa | Marcel Leroux | Springer.
718 [online] Available from: http://www.springer.com/us/book/9783540426363 (Accessed 14
719 December 2015), 2001.

720 Lézine, A.-M., Duplessy, J.-C. and Cazet, J.-P.: West African monsoon variability during the
721 last deglaciation and the Holocene: Evidence from fresh water algae, pollen and isotope data
722 from core KW31, Gulf of Guinea, Palaeogeography, Palaeoclimatology, Palaeoecology,
723 219(3–4), 225–237, doi:10.1016/j.palaeo.2004.12.027, 2005.

724 Lézine, A.-M., Holl, A. F.-C., Lebamba, J., Vincens, A., Assi-Khaudjis, C., Février, L. and
725 Sultan, É.: Temporal relationship between Holocene human occupation and vegetation change
726 along the northwestern margin of the Central African rainforest, Comptes Rendus Geoscience,
727 345(7–8), 327–335, doi:10.1016/j.crte.2013.03.001, 2013.

728 Loomis, S. E., Russell, J. M., Ladd, B., Street-Perrott, F. A. and Sinninghe Damsté, J. S.:
729 Calibration and application of the branched GDGT temperature proxy on East African lake
730 sediments, Earth and Planetary Science Letters, 357–358, 277–288,
731 doi:10.1016/j.epsl.2012.09.031, 2012.

732 Marret, F. and Kim, S.-Y.: Operculodinium aguinawense sp. nov., A Dinoflagellate Cyst from
733 the Late Pleistocene and Recent Sediments of the East Equatorial Atlantic Ocean, Palynology,
734 33(1), 125–139, doi:10.2113/gspalynol.33.1.125, 2009.

735 Marret, F. and Zonneveld, K. A. F.: Atlas of modern organic-walled dinoflagellate cyst
736 distribution, Review of Palaeobotany and Palynology, 125(1–2), 1–200, doi:10.1016/S0034-
737 6667(02)00229-4, 2003.

738 Marret, F., Maley, J. and Scourse, J.: Climatic instability in west equatorial Africa during the
739 Mid- and Late Holocene, Quaternary International, 150(1), 71–81,
740 doi:10.1016/j.quaint.2006.01.008, 2006.

741 Marret, F., Scourse, J., Kennedy, H., Ufkes, E. and Jansen, J. H. F.: Marine production in the
742 Congo-influenced SE Atlantic over the past 30,000 years: A novel dinoflagellate-cyst based
743 transfer function approach, Marine Micropaleontology, 68(1–2), 198–222,
744 doi:10.1016/j.marmicro.2008.01.004, 2008.

745 Marret, F., Kim, S.-Y. and Scourse, J.: A 30,000 yr record of land–ocean interaction in the
746 eastern Gulf of Guinea, Quaternary Research, 80(1), 1–8, doi:10.1016/j.yqres.2013.04.003,
747 2013.

748 McGee, D., Donohoe, A., Marshall, J. and Ferreira, D.: Changes in ITCZ location and cross-
749 equatorial heat transport at the Last Glacial Maximum, Heinrich Stadial 1, and the mid-
750 Holocene, Earth and Planetary Science Letters, 390, 69–79, doi:10.1016/j.epsl.2013.12.043,
751 2014.

752 Merlis, T. M., Schneider, T., Bordoni, S. and Eisenman, I.: The Tropical Precipitation
753 Response to Orbital Precession, J. Climate, 26(6), 2010–2021, doi:10.1175/JCLI-D-12-
754 00186.1, 2012.

Mix, A. C., Bard, E. and Schneider, R.: Environmental processes of the ice age: land, oceans, glaciers (EPILOG), Quaternary Science Reviews, 20(4), 627–657, doi:10.1016/S0277-3791(00)00145-1, 2001.

Müller, P. J., Kirst, G., Ruhland, G., von Storch, I. and Rosell-Melé, A.: Calibration of the alkenone paleotemperature index U37K′ based on core-tops from the eastern South Atlantic and the global ocean (60°N-60°S), Geochimica et Cosmochimica Acta, 62(10), 1757–1772, doi:10.1016/S0016-7037(98)00097-0, 1998.

Nicholson, S. E.: A revised picture of the structure of the "monsoon" and land ITCZ over West Africa, Clim Dyn, 32(7–8), 1155–1171, doi:10.1007/s00382-008-0514-3, 2009.

Picot, M., Droz, L., Marsset, T., Dennielou, B. and Bez, M.: Controls on turbidite sedimentation: Insights from a quantitative approach of submarine channel and lobe architecture (Late Quaternary Congo Fan), Marine and Petroleum Geology, 72, 423–446, doi:10.1016/j.marpetgeo.2016.02.004, 2016.

Powers, L. A., Johnson, T. C., Werne, J. P., Castañeda, I. S., Hopmans, E. C., Sinninghe Damsté, J. S. and Schouten, S.: Large temperature variability in the southern African tropics since the Last Glacial Maximum, Geophys. Res. Lett., 32(8), L08706, doi:10.1029/2004GL022014, 2005.

Prance, G. T.: The vegetation of Africa. by F. White, Brittonia, 36(3), 273–273, doi:10.2307/2806524, 1984.

Radi, T. and de Vernal, A.: Dinocysts as proxy of primary productivity in mid–high latitudes of the Northern Hemisphere, Marine Micropaleontology, 68(1–2), 84–114, doi:10.1016/j.marmicro.2008.01.012, 2008.

Reimer, P.: IntCal13 and Marine13 Radiocarbon Age Calibration Curves 0–50,000 Years cal BP, Radiocarbon, 55(4), 1869–1887, doi:10.2458/azu_js_rc.55.16947, 2013.

Savoye, B.: Zaiango 1 cruise report mission, , doi:10.17600/98010100, 1998.

Savoye, B., Cochonat, P., Apprioual, R., Bain, O., Baltzer, A., Bellec, V., Beuzart, P., Bourillet, J.-F., Cagna, R., Cremer, M., Crusson, A., Dennielou, B., Diebler, D., Droz, L., Ennes, J.-C., Floch, G., Guiomar, M., Harmegnies, F., Kerbrat, R., Klein, B., Kuhn, H., Landuré, J.-Y., Lasnier, C., Le Drezen, E., Le Formal, J.-P., Lopez, M., Loubrieu, B., Marsset, T., Migeon, S., Normand, A., Nouzé, H., Ondréas, H., Pelleau, P., Saget, P., Séranne, M., Sibuet, J.-C., Tofani, R. and Voisset, M.: Structure et évolution récente de l'éventail turbiditique du Zaïre : premiers résultats scientifiques des missions d'exploration Zaïango1 and 2 (marge Congo–Angola), Comptes Rendus de l'Académie des Sciences - Series IIA - Earth and Planetary Science, 331(3), 211–220, doi:10.1016/S1251-8050(00)01385-9, 2000.

Savoye, B., Babonneau, N., Dennielou, B. and Bez, M.: Geological overview of the Angola–Congo margin, the Congo deep-sea fan and its submarine valleys, Deep Sea Research Part II: Topical Studies in Oceanography, 56(23), 2169–2182, doi:10.1016/j.dsr2.2009.04.001, 2009.

Schefuß, E., Schouten, S. and Schneider, R. R.: Climatic controls on central African hydrology during the past 20,000 years, Nature, 437(7061), 1003–1006, doi:10.1038/nature03945, 2005.

795 Schneider, R. R., Price, B., Müller, P. J., Kroon, D. and Alexander, I.: Monsoon related
796 variations in Zaire (Congo) sediment load and influence of fluvial silicate supply on marine
797 productivity in the east equatorial Atlantic during the last 200,000 years, Paleoceanography,
798 12(3), 463–481, doi:10.1029/96PA03640, 1997.

799 Shakun, J. D. and Carlson, A. E.: A global perspective on Last Glacial Maximum to Holocene
800 climate change, Quaternary Science Reviews, 29(15–16), 1801–1816,
801 doi:10.1016/j.quascirev.2010.03.016, 2010.

802 Shanahan, T. M., Beck, J. W., Overpeck, J. T., McKay, N. P., Pigati, J. S., Peck, J. A., Scholz,
803 C. A., Heil Jr., C. W. and King, J.: Late Quaternary sedimentological and climate changes at
804 Lake Bosumtwi Ghana: New constraints from laminae analysis and radiocarbon age
805 modeling, Palaeogeography, Palaeoclimatology, Palaeoecology, 361–362, 49–60,
806 doi:10.1016/j.palaeo.2012.08.001, 2012.

807 Shanahan, T. M., McKay, N. P., Hughen, K. A., Overpeck, J. T., Otto-Bliesner, B., Heil, C. W.,
808 King, J., Scholz, C. A. and Peck, J.: The time-transgressive termination of the African Humid
809 Period, Nature Geosci, 8(2), 140–144, doi:10.1038/ngeo2329, 2015.

810 Shi, N., Dupont, L. M., Beug, H.-J. and Schneider, R.: Vegetation and climate changes during
811 the last 21 000 years in S.W. Africa based on a marine pollen record, Veget Hist Archaebot,
812 7(3), 127–140, doi:10.1007/BF01374001, 1998.

813 Stager, J. C., Mayewski, P. A. and Meeker, L. D.: Cooling cycles, Heinrich event 1, and the
814 desiccation of Lake Victoria, Palaeogeography, Palaeoclimatology, Palaeoecology, 183(1–2),
815 169–178, doi:10.1016/S0031-0182(01)00468-0, 2002.

816 Stager, J. C., Ryves, D. B., Chase, B. M. and Pausata, F. S. R.: Catastrophic Drought in the
817 Afro-Asian Monsoon Region During Heinrich Event 1, Science, 331(6022), 1299–1302,
818 doi:10.1126/science.1198322, 2011.

819 Svensson, A., Andersen, K. K., Bigler, M., Clausen, H. B., Dahl-Jensen, D., Davies, S. M.,
820 Johnsen, S. J., Muscheler, R., Parrenin, F., Rasmussen, S. O., Röthlisberger, R., Seierstad, I.,
821 Steffensen, J. P. and Vinther, B. M.: A 60 000 year Greenland stratigraphic ice core
822 chronology, Clim. Past, 4(1), 47–57, doi:10.5194/cp-4-47-2008, 2008.

823 Weldeab, S., Schneider, R.R., Kölling, M., Wefer, G.,: Holocene African droughts relate to
824 eastern equatorial Atlantic cooling. Geology, Geology, 33(12), doi:10.1130/G21874.1, 2005.

825 Tierney, J. E. and deMenocal, P. B.: Abrupt Shifts in Horn of Africa Hydroclimate Since the
826 Last Glacial Maximum, Science, 342(6160), 843–846, doi:10.1126/science.1240411, 2013.

827 Tierney, J. E., Russell, J. M., Sinninghe Damsté, J. S., Huang, Y. and Verschuren, D.: Late
828 Quaternary behavior of the East African monsoon and the importance of the Congo Air
829 Boundary, Quaternary Science Reviews, 30(7–8), 798–807,
830 doi:10.1016/j.quascirev.2011.01.017, 2011.

831 Tuenter, E., Weber, S. L., Hilgen, F. J. and Lourens, L. J.: The response of the African summer
832 monsoon to remote and local forcing due to precession and obliquity, Global and Planetary
833 Change, 36(4), 219–235, doi:10.1016/S0921-8181(02)00196-0, 2003.

834 Voituriez, B.: Les sous-courants équatoriaux nord et sud et la formation des dômes thermiques

tropicaux, Oceanologica Acta, 4(4), 497–506, 1981.

Walker, M. J. C., Berkelhammer, M., Björck, S., Cwynar, L. C., Fisher, D. A., Long, A. J., Lowe, J. J., Newnham, R. M., Rasmussen, S. O. and Weiss, H.: Formal subdivision of the Holocene Series/Epoch: a Discussion Paper by a Working Group of INTIMATE (Integration of ice-core, marine and terrestrial records) and the Subcommission on Quaternary Stratigraphy (International Commission on Stratigraphy), J. Quaternary Sci., 27(7), 649–659, doi:10.1002/jqs.2565, 2012.

Weijers, J. W. H., Schefuß, E., Schouten, S. and Damsté, J. S. S.: Coupled Thermal and Hydrological Evolution of Tropical Africa over the Last Deglaciation, Science, 315(5819), 1701–1704, doi:10.1126/science.1138131, 2007.

Weldeab, S.: Bipolar modulation of millennial-scale West African monsoon variability during the last glacial (75,000–25,000 years ago), Quaternary Science Reviews, 40, 21–29, doi:10.1016/j.quascirev.2012.02.014, 2012.

Weldeab, S., Lea, D. W., Schneider, R. R. and Andersen, N.: 155,000 Years of West African Monsoon and Ocean Thermal Evolution, Science, 316(5829), 1303–1307, doi:10.1126/science.1140461, 2007.

Zarriess, M. and Mackensen, A.: The tropical rainbelt and productivity changes off northwest Africa: A 31,000-year high-resolution record, Marine Micropaleontology, 76(3–4), 76–91, doi:10.1016/j.marmicro.2010.06.001, 2010.

Zonneveld, K. A. F., Marret, F., Versteegh, G. J. M., Bogus, K., Bonnet, S., Bouimetarhan, I., Crouch, E., de Vernal, A., Elshanawany, R., Edwards, L., Esper, O., Forke, S., Grøsfjeld, K., Henry, M., Holzwarth, U., Kielt, J.-F., Kim, S.-Y., Ladouceur, S., Ledu, D., Chen, L., Limoges, A., Londeix, L., Lu, S.-H., Mahmoud, M. S., Marino, G., Matsouka, K., Matthiessen, J., Mildenhal, D. C., Mudie, P., Neil, H. L., Pospelova, V., Qi, Y., Radi, T., Richerol, T., Rochon, A., Sangiorgi, F., Solignac, S., Turon, J.-L., Verleye, T., Wang, Y., Wang, Z. and Young, M.: Atlas of modern dinoflagellate cyst distribution based on 2405 data points, Review of Palaeobotany and Palynology, 191, 1–197, doi:10.1016/j.revpalbo.2012.08.003, 2013.

9. TABLE AND FIGURE CAPTIONS

9.1. Table caption

Table 1 : ^{14}C dates obtained on KZAI-01 core: seven dates were previously obtained on marine carbonate material and 10 on bulk organic matter (Bayon et al., 2012), and three new dates have been added in this study. Two dates have been rejected (190 and 372 cm) and displayed in italic, and dates acquired on bulk organic matter have not been considered for the age model establishment in this study (dates retained for the age model in bold in the Table).

9.2. Figure captions

Figure 1: Map showing locations of KZAI-01 core and other cores mentioned in the text: GeoB6518 (Schefuß et al., 2005; Bayon et al., 2012), GeoB1008 (Schneider et al., 1997), MD32-2707 (Weldeab et al., 2007), GeoB1023 (Shi et al., 1998), and GITANGA2 (Bonnefille and Chalié, 2000). The general pattern of present-day surface ocean currents of the adjacent Atlantic Ocean is extracted from Lass and Mohrholz (2008) and includes: the Guinea Current (GC), the northern (nSEC), equatorial (eSEC), central (cSEC), and southern (sSEC) South Equatorial Current, the Angola Current (AC), the Angola-Benguela Front (ABF), the Benguela Current (BC) and the Agulhas Current (AgC). Orange lines indicate warm currents and blue lines cold currents. Green zones correspond to upwelling zone (BUS : Benguela Upwelling System) and oceanic domes (AD : Angola Dome, ED : Equatorial Dome; Voituriez, 1981; Lass and Mohrholz, 2008). Black dashed lines display mean seasonal locations of the ITCZ during July and January (Collier and Hughes, 2011). Red 5°C-interval isolines correspond to annual mean SST (Hirahara et al., 2013). Vegetation cover (in % per surface unity) is extracted from Hansen et al. (2013) dataset.

Figure 2: Age model established through a linear regression between retained AMS ^{14}C pointers (red squares; cf. Table 1). Blue squares correspond to ^{14}C datations acquired on organic matter (Bayon et al., 2012), not taken into account for the age model. Green squares correspond to dates obtained by tuning KZAI-01 core with GeoB6518 core, on the basis on similar XRF Ti / Ca ratio trends. Grey band corresponds to the 2 σ range error of calibrated dates, and purple lines correspond to sedimentation rates (cm/ky).

Figure 3: Comparison between total dinocyst concentrations (cysts / cm^3), non-heterotrophic cyst concentrations, as well as *Lingulodinium machaerophorum* and *Operculodinium centrocarpum* concentrations, both species being mainly responsible for total cyst concentrations in the study core. Same approach for heterotrophic taxa: comparison between total heterotrophic concentrations in parallel with *Brigantedinium* spp. and *Echinidinium* spp., both taxa being mainly responsible for total heterotrophic concentrations in the study core. Above mentioned species are also represented in cumulated percentages. To discuss relationships between primary productivity, dinocyst concentrations and terrigenous dilution, the XRF Ti/Ca ratio of core KZAI-01 is displayed in parallel with biogenic opal and total organic matter signals extracted from core GeoB1008 (Schneider et al., 1997). Also, specific diversity and dominance indexes enable discussing the potential advection of dinocysts in the study. Red dashed lines correspond to major transitions in total dinocyst concentrations allowing to define 5 major palynozones (A-B-C-D-E).

Figure 4: Selection of major (>2%) non-heterotrophic dinocyst species represented in percentages, in parallel with total non-heterotrophic cyst concentrations (cysts / cm^3). Some species have been grouped: *Spiniferites ramosus* also includes *Spiniferites bulloides*, and *Nematosphaeropsis labyrinthus* also includes *Nematosphaeropsis lemniscata*. Palynozones (A to E) have been established according to major variations in absolute cyst concentrations (cf. Figure 3), and minor subdivisions (Ax-Ex) have been delimited thanks to whole dinocyst assemblages in percentages (cf. Figures 4 and 5). Species are here classified according to observed temporal successions underlined by black arrows.

Figure 5: Selection of major (>2%) heterotrophic dinocyst species represented in percentages, in parallel with total heterotrophic cyst concentrations (cysts / cm^3). *Echinidinium* spp. includes *E. aculeatum, E. delicatum, E. granulatum* and *E. transparantum*. *Lingulodinium machaerophorum* is displayed with *Echinidinium* spp. regarding their river-plume affinity. Palynozones (A to E) have been established according to major variations in absolute cyst concentrations (cf. Figure 3), and minor subdivisions (Ax-Ex) have been delimited thanks to whole dinocyst assemblages in percentages (cf. Figures 4 and 5). Species are here classified according to observed temporal successions underlined by black arrows.

Figure 6: Present-day distribution of selected dinocyst taxa among major ones discussed in the paper. Percentages from 277 sites are extracted from the modern dinocyst atlas (Marret et al., 2008; Zonneveld et al., 2013).

Figure 7: Comparison between total heterotrophic cyst abundances and *Trinovantedinium applanatum* percentages, both accounting for upwelling activity (Marret and Zonneveld, 2003). River-plume taxa: *Echinidinium* spp. and *Lingulodinium machaerophorum,* as well as coenobia of freshwater microalgae *Pediastrum* and terrigenous signals (XRF Ti/Ca ratio, quantitative measurements of major elements Al/K and Al/Si; Bayon et al., 2012), allow discussing Congo River discharges. Relationships between river discharges and paleomonsoons are displayed throughout : i) pollen-inferred rainfall anomalies in Burundi mounts (Bonnefille and Chalié, 2000: the threshold with positive anomalies in green and negative anomalies in orange is calculated from mean glacial values) in parallel with δD on Alkane C_{29} (core GeoB6518; Schefuß) displayed in red, ii) regional-scale monsoon reconstructions (Western and Eastern African Monsoons; Caley et al., 2011: maximal monsoon regimes are underlined in green), iii) *Globigerinoides ruber* Ba/Ca ratio obtained from core MD32-2707 (Weldeab et al., 2007). Orbital parameters such as the Obliquity and the Precession (Berger and Loutre, 1991) are also displayed with precession minima and obliquity maxima highlighted in green. Green bands correspond to major orbital-scale moisture conditions discussed in the paper.

Figure 8: Temporal focus on the last 20 ky. Sea-surface temperature changes are discussed with major dinocyst species classified according to their trophic affinity: *Spiniferites mirabilis*, *Spiniferites membranaceus*, *Selenopemphix nephroides* and *Stelladinium reidii*. Sea-surface salinity changes are discussed with *Echinidinium* spp., *Operculodinium aguinawense*, *Lingulodinium machaerophorum*, in addition with stable isotopic signals from core GeoB6518-1 (Schefuß et al., 2005). Upwelling activity and Benguela Current activity are respectively discussed in KZAI-01 core with *Trinovantedinium applanatum* and *Operculodinium centrocarpum* percentages, together with latitudinal location of the Angola-Benguela Front (Jansen et al., 1996) and *O. Centrocarpum* relative abundances acquired in the Benguela Upwelling System on GeoB1023 core (Shi et al., 1998). Higher primary

productivity conditions in the study area are indirectly discussed with *Brigantedinium* spp. percentages. XRF Ti/Ca ratio obtained on KZAI-01 core allows discussing past terrigenous supplies. NGRIP $\delta^{18}O$ (GICC05 timescale; Svensson et al., 2008) is also displayed in parallel with the Last Deglaciation - Holocene (Walker et al., 2012) subdivisions : Last Glacial Maximum (LGM), Heinrich Stadial 1 (HS1), Bølling-Allerød (B/A), Younger Dryas (YD), Early Holocene (EH), Mid-Holocene (MH), and Late Holocene (LH). Blue bands correspond to cold and dry events recorded with dinocyst assemblages. African Humid Period (AHP) terminations are also depicted according to the literature (orange bars) : 1°(Kröpelin et al., 2008), 2° (Shanahan et al., 2015), 3° (Hély et al., 2009), 4°(Lézine et al., 2005), 5°(Lebamba et al., 2012), 6°(Lézine et al., 2013), 7°(Tierney and deMenocal, 2013), 8°(Shanahan et al., 2012), 9° (deMenocal et al., 2000). Palynozones subdivisions are also highlighted (aX, bX; cf. Figures 4 and 5).

Depth (cm)	Material dated	Laboratory number	^{14}C age (BP)	Mean calibrated age (cal BP) +/- 2σ range	Data origin
10	**Mixed marine carbonate**	**UtC-9311**	**2,172 +/- 39**	**1,735 +/- 82**	**Bayon et al., 2012**
13	Bulk organic matter	Poz-40293	1,610 +/- 30	1,170 +/ -82	Bayon et al., 2012
18	Bulk organic matter	Poz-40295	2,310 +/- 30	1,921 +/ -91	Bayon et al., 2012
26	Bulk organic matter	Poz-40296	2,545 +/- 30	2,216 +/ -89	Bayon et al., 2012
37	Bulk organic matter	Poz-40297	3,210 +/- 30	3,024 +/- 112	Bayon et al., 2012
51	Bulk organic matter	Poz-40298	3,770 +/- 30	3,713 +/- 103	Bayon et al., 2012
70	Bulk organic matter	Poz-40299	4,435 +/- 35	4,636 +/- 138	Bayon et al., 2012
122	Bulk organic matter	Poz-40300	5,970 +/- 40	6,380 +/- 94	Bayon et al., 2012
190	*Mixed marine carbonate*	*UtC-9312*	*8,710 +/- 60*	*9,369 +/ -131*	*Bayon et al., 2012*
196	Bulk organic matter	Poz-40301	8,080 +/- 40	8,527 +/- 110	Bayon et al., 2012
269	Bulk organic matter	Poz-40302	9,790 +/- 50	10,727 +/- 166	Bayon et al., 2012
305	Bulk organic matter	Poz-40389	10,400 +/-60 50	11,503 +/- 252	Bayon et al., 2012
356	**Planktonic foraminifera**	**Poz-20108**	**10,930 +/-50**	**12,444 +/- 175**	**Bayon et al., 2012**
372	*Bivalve*	*Poz-73781*	*13,450 +/-70*	*15,598 +/- 276*	*This paper*
456	**Planktonic foraminifera**	**Poz-20109**	**13,950 +/-70**	**16,328 +/- 251**	**Bayon et al., 2012**
522	***Bolivina spatulatha***	**Poz-73782**	**20,800+/-140**	**24,575 +/- 446**	**This paper**
585	**Planktonic foraminifera**	**Poz-20110**	**23,020 +/-130**	**27,232 +/- 689**	**Bayon et al., 2012**
622	**Bivalve**	**Poz-73783**	**24,870+/- 200**	**28,454 +/- 447**	**This paper**
678	**Mixed marine carbonate**	**UtC-9314**	**28,240+/-280**	**31,812 +/- 668**	**Bayon et al., 2012**
851	**Mixed marine carbonate**	**UtC-9315**	**31,800+/-400**	**35,274 +/- 405**	**Bayon et al., 2012**

Table 1

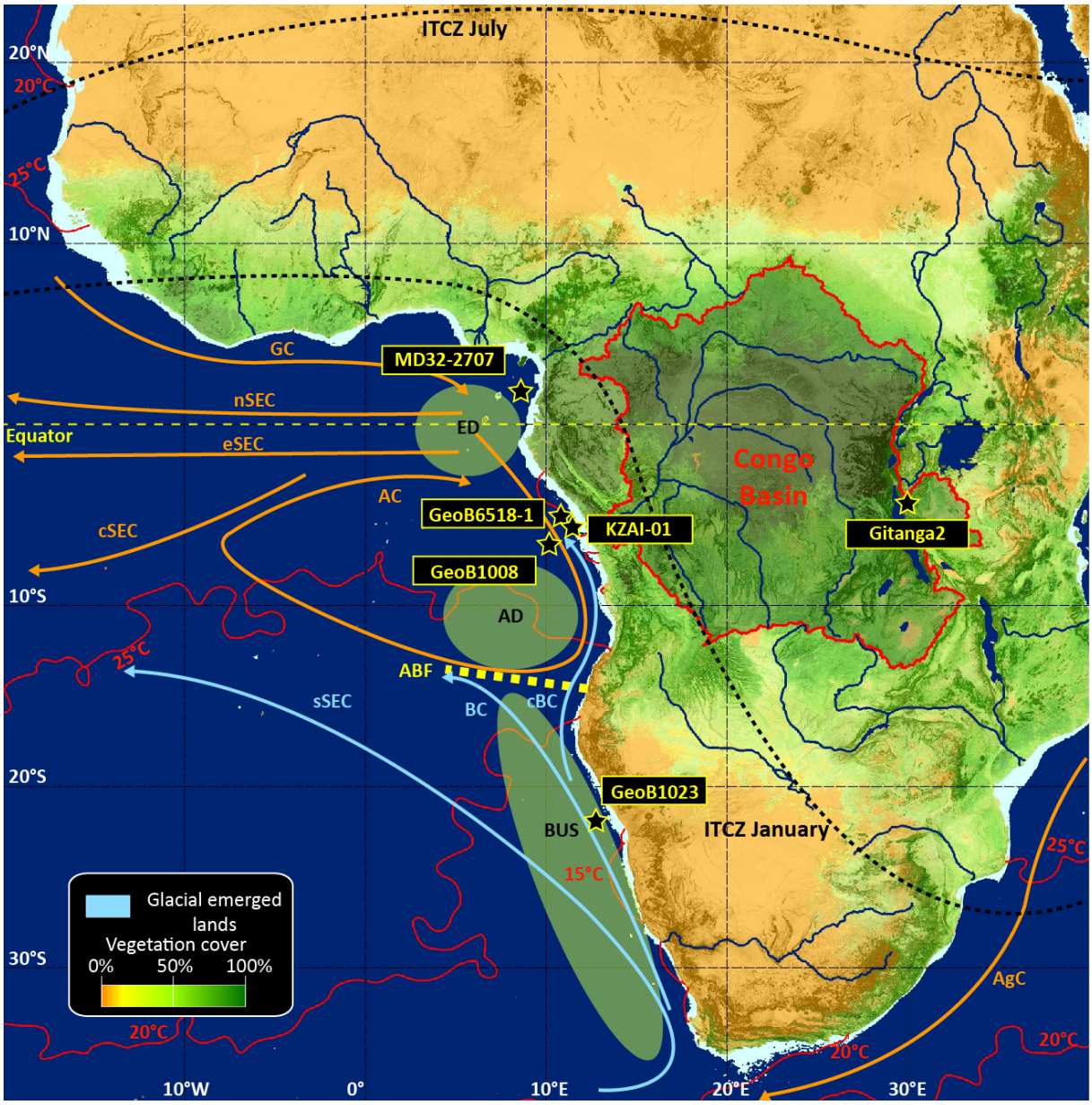
ITCZ July
20°N
20°C
25°C
10°N
GC
MD32-2707
nSEC
Equator
eSEC
ED
AC
GeoB6518-1
KZAI-01
Congo Basin
Gitanga2
cSEC
GeoB1008
10°S
AD
25°C
ABF
sSEC
BC
cBC
20°S
GeoB1023
BUS
ITCZ January
15°C
25°C
Glacial emerged lands
Vegetation cover
0%
50%
100%
30°S
AgC
20°C
20°C
20°C
10°W
0°
10°E
20°E
30°E

Figure 1

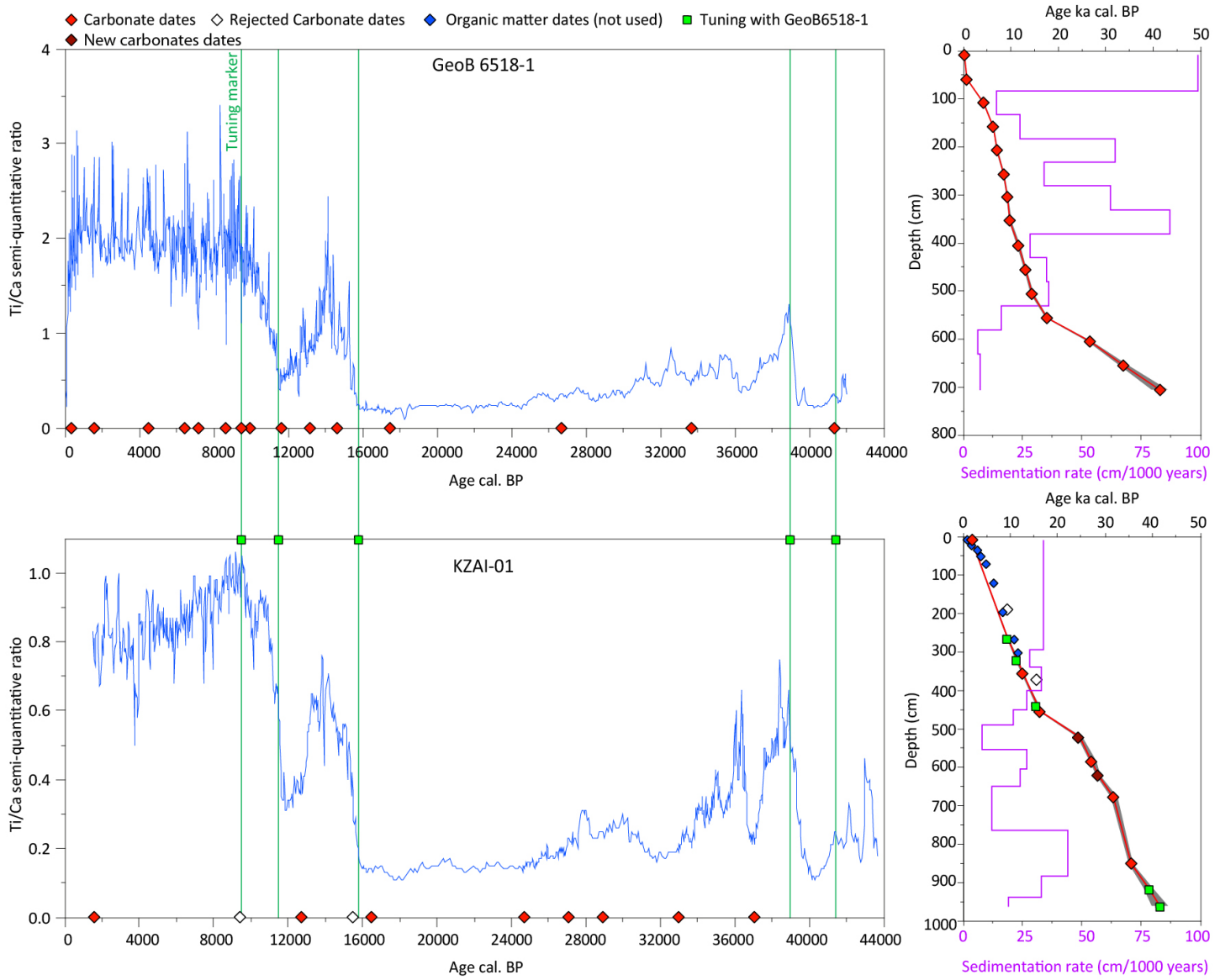

1035 **Figure 2**
1036

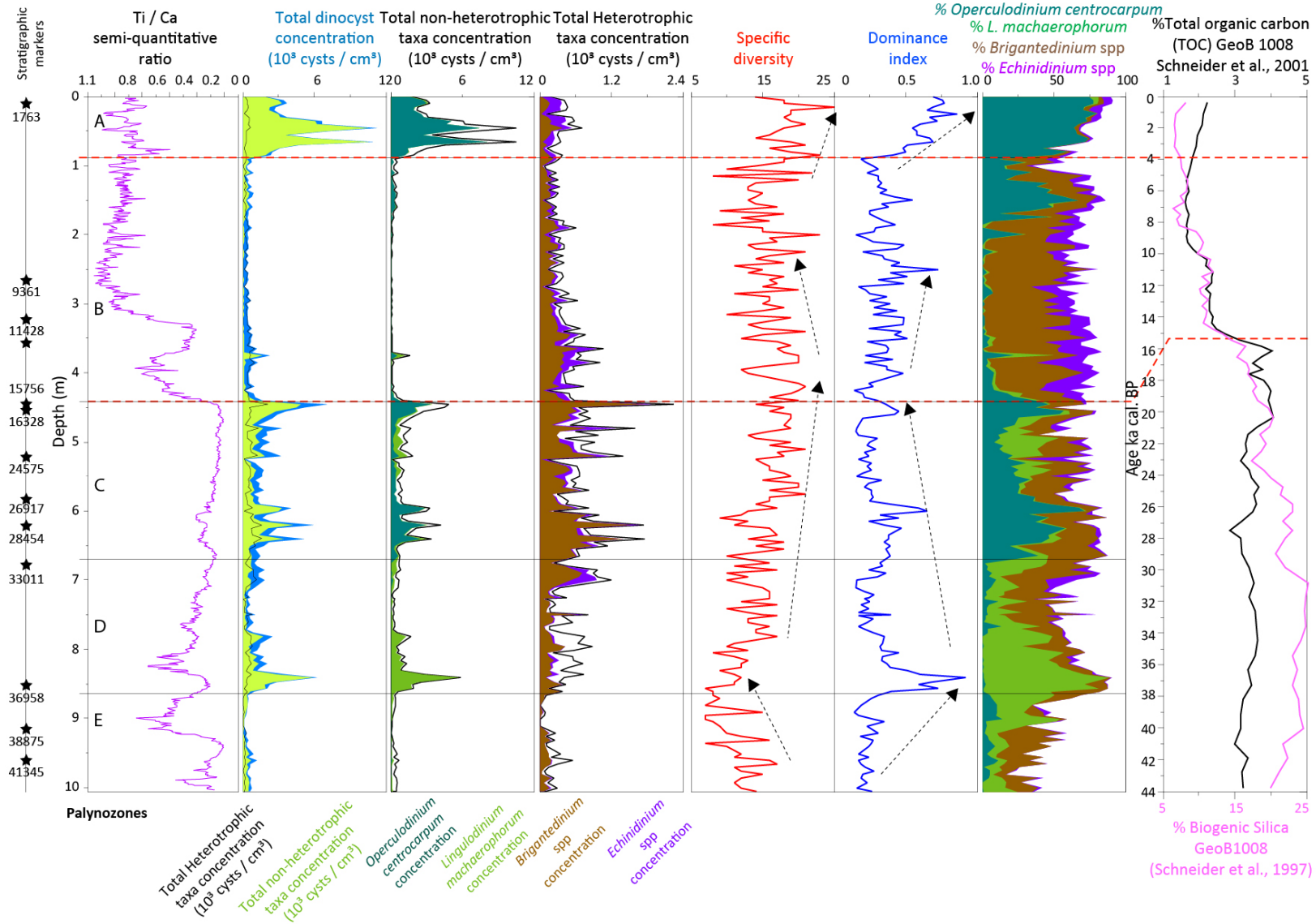
Stratigraphic markers
Ti / Ca semi-quantitative ratio
Total dinocyst concentration (10³ cysts / cm³)
Total non-heterotrophic taxa concentration (10³ cysts / cm³)
Total Heterotrophic taxa concentration (10³ cysts / cm³)
Specific diversity
Dominance index
% Operculodinium centrocarpum
% L. machaerophorum
% Brigantedinium spp
% Echinidinium spp
%Total organic carbon (TOC) GeoB 1008 Schneider et al., 2001
Depth (m)
Age ka cal. BP
1763
9361
11428
15756
16328
24575
26917
28454
33011
36958
38875
41345
A
B
C
D
E
Palynozones
Total Heterotrophic taxa concentration (10³ cysts / cm³)
Total non-heterotrophic taxa concentration (10³ cysts / cm³)
Operculodinium centrocarpum concentration
Lingulodinium machaerophorum concentration
Brigantedinium spp concentration
Echinidinium spp concentration
% Biogenic Silica GeoB1008 (Schneider et al., 1997)

Figure 3

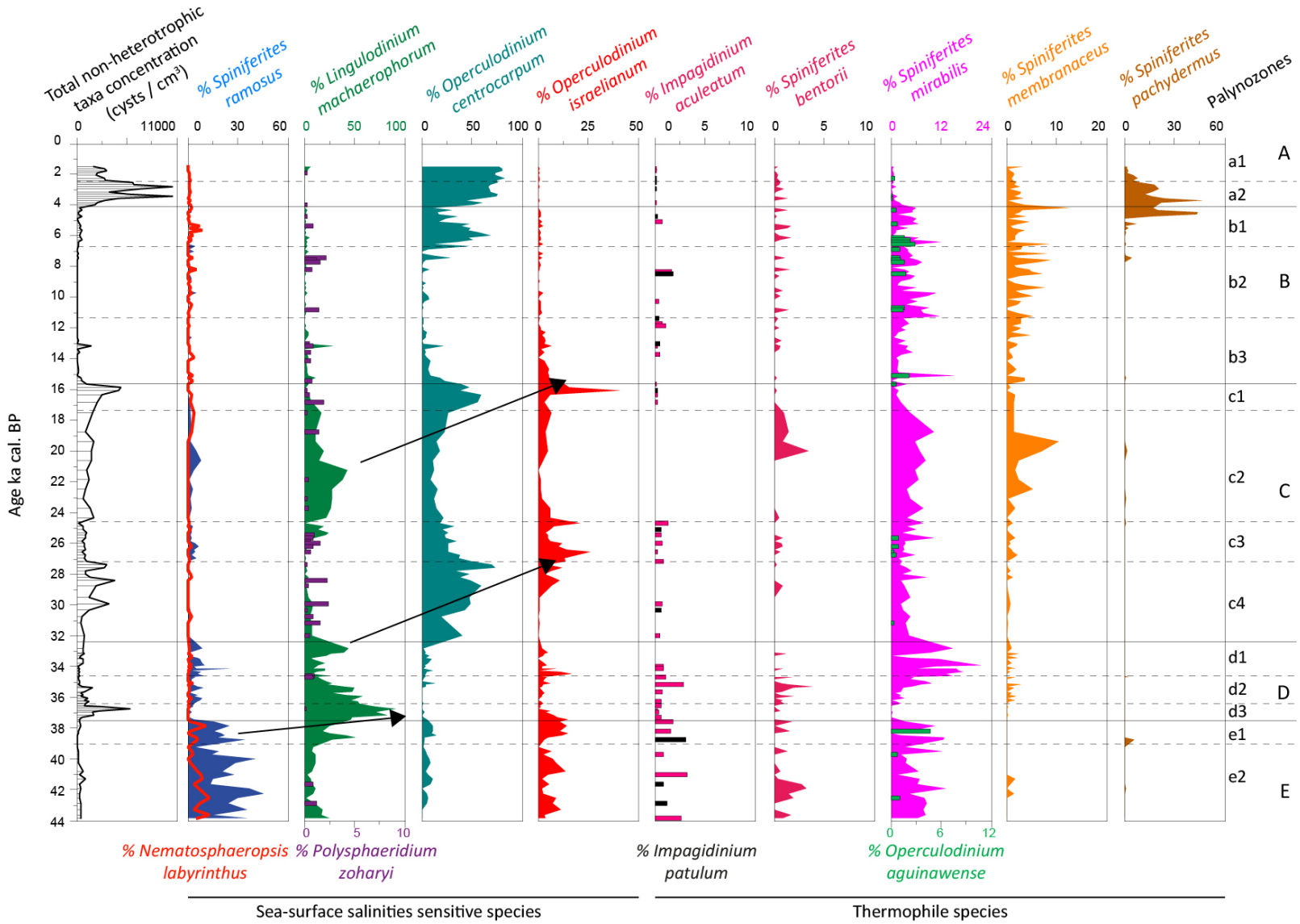
Total non-heterotrophic taxa concentration (cysts / cm³)
% Spiniferites ramosus
% Lingulodinium machaerophorum
% Operculodinium centrocarpum
% Operculodinium israelianum
% Impagidinium aculeatum
% Spiniferites bentorii
% Spiniferites mirabilis
% Spiniferites membranaceus
% Spiniferites pachydermus
Palynozones
Age ka cal. BP
a1
a2
b1
b2
b3
c1
c2
c3
c4
d1
d2
d3
e1
e2
A
B
C
D
E
% Nematosphaeropsis labyrinthus
% Polysphaeridium zoharyi
% Impagidinium patulum
% Operculodinium aguinawense
Sea-surface salinities sensitive species
Thermophile species

Figure 4

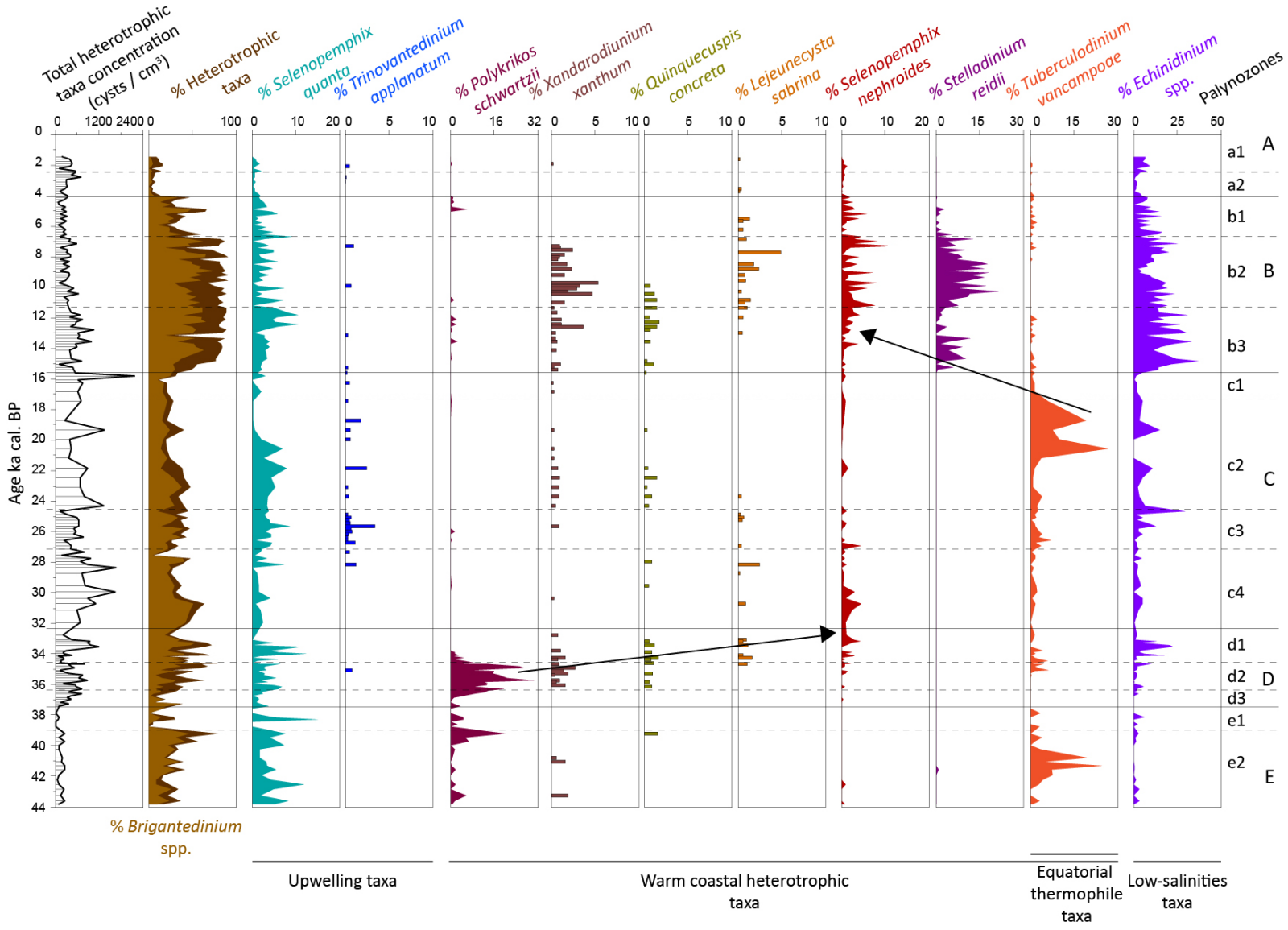
Total heterotrophic taxa concentration (cysts / cm³)
% Heterotrophic taxa
% Selenopemphix quanta
% Trinovantedinium applanatum
% Polykrikos schwartzii
% Xandarodiunium xanthum
% Quinquecuspis concreta
% Lejeunecysta sabrina
% Selenopemphix nephroides
% Stelladinium reidii
% Tuberculodinium vancampoae
% Echinidinium spp.
Palynozones
Age ka cal. BP
a1
a2
b1
b2
b3
c1
c2
c3
c4
d1
d2
d3
e1
e2
A
B
C
D
E
% Brigantedinium spp.
Upwelling taxa
Warm coastal heterotrophic taxa
Equatorial thermophile taxa
Low-salinities taxa

Figure 5

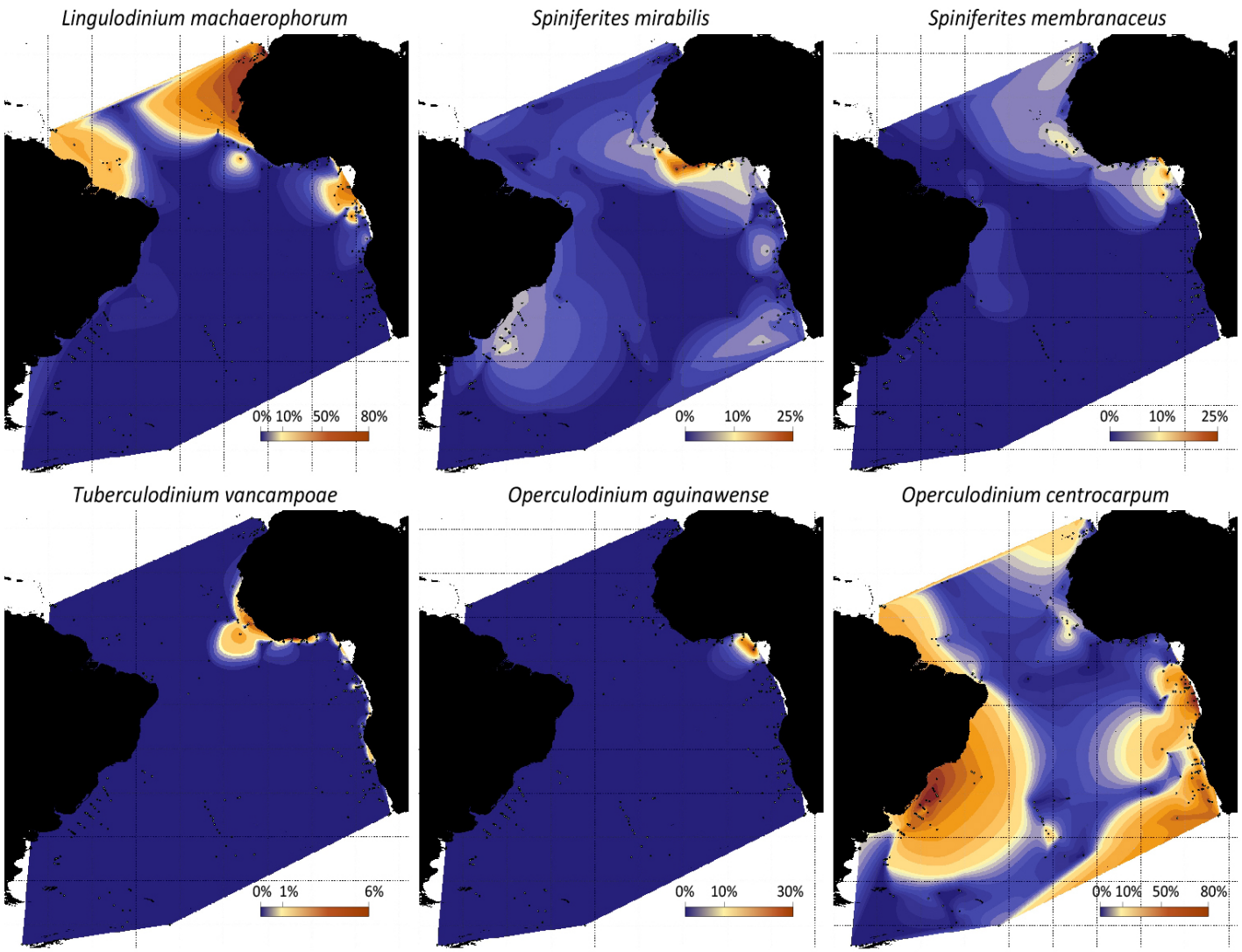

1043
1044 **Figure 6**

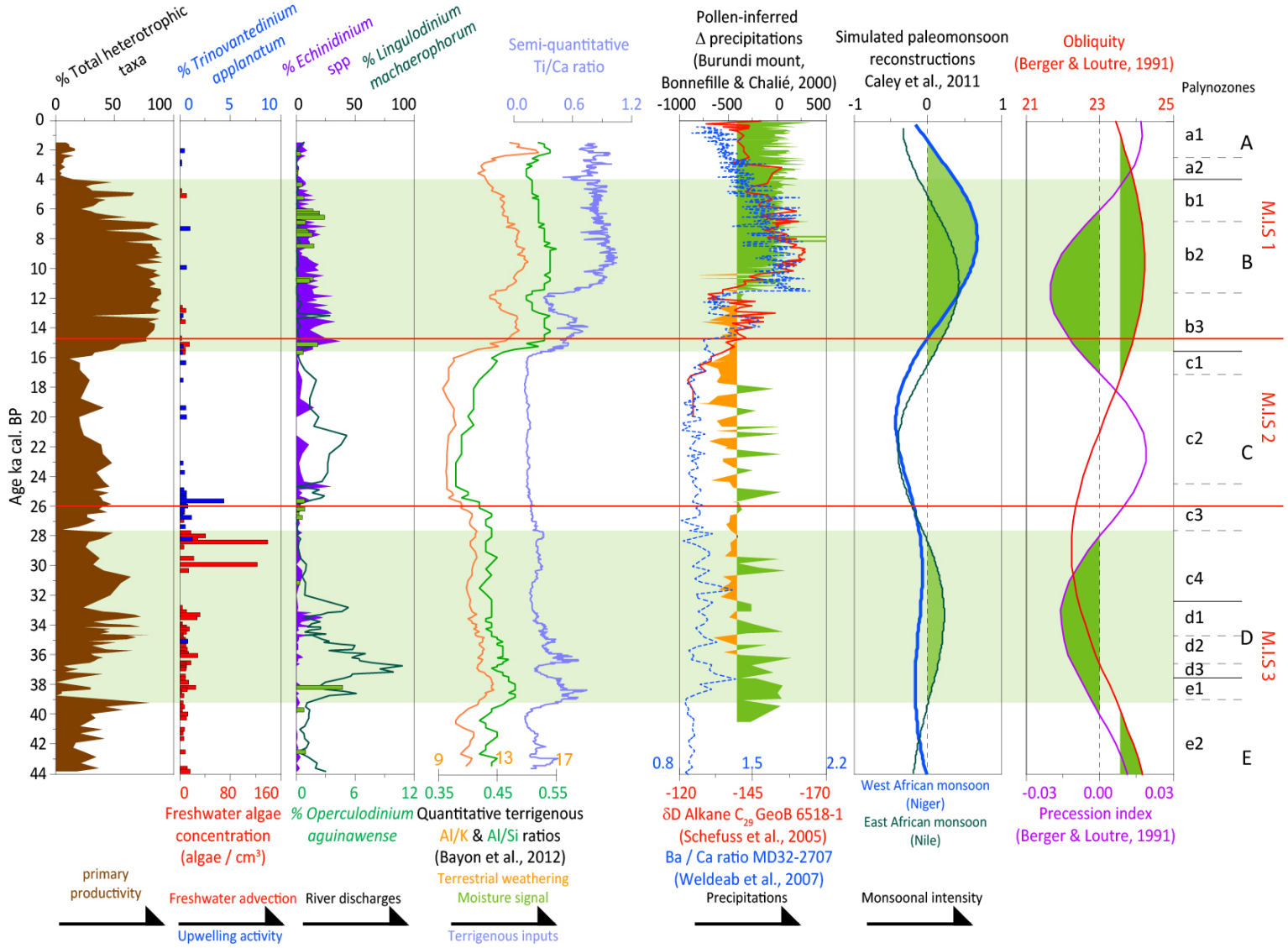
% Total heterotrophic taxa
% Trinovantedinium applanatum
% Echinidinium spp
% Lingulodinium machaerophorum
Semi-quantitative Ti/Ca ratio
Pollen-inferred Δ precipitations (Burundi mount, Bonnefille & Chalié, 2000)
Simulated paleomonsoon reconstructions Caley et al., 2011
Obliquity (Berger & Loutre, 1991)
Palynozones
Age ka cal. BP
Freshwater algae concentration (algae / cm³)
% Operculodinium aguinawense
Quantitative terrigenous Al/K & Al/Si ratios (Bayon et al., 2012)
δD Alkane C29 GeoB 6518-1 (Schefuss et al., 2005)
Ba / Ca ratio MD32-2707 (Weldeab et al., 2007)
West African monsoon (Niger)
East African monsoon (Nile)
Precession index (Berger & Loutre, 1991)
primary productivity
Freshwater advection
River discharges
Terrestrial weathering
Moisture signal
Precipitations
Monsoonal intensity
Upwelling activity
Terrigenous inputs
M.I.S 1
M.I.S 2
M.I.S 3

Figure 7

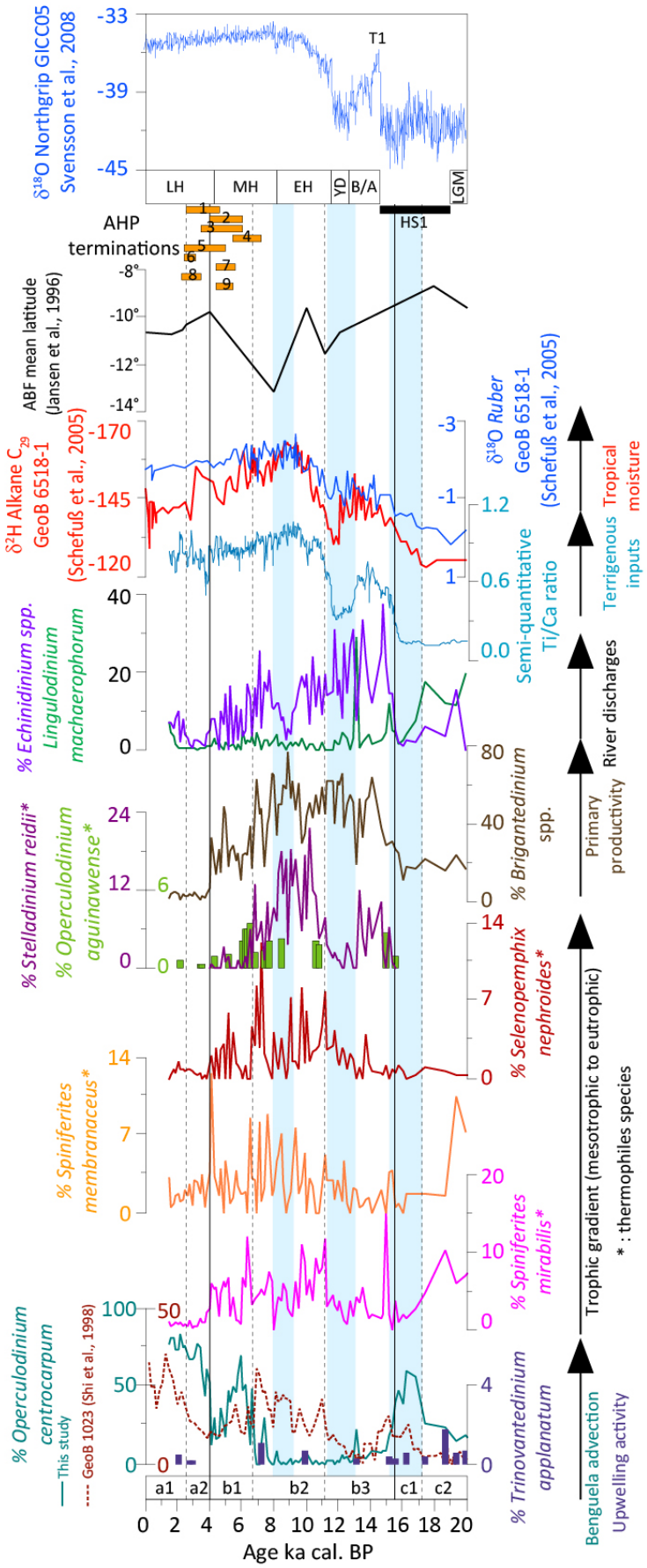
δ18O Northgrip GICC05 Svensson et al., 2008
T1
LH
MH
EH
YD
B/A
LGM
HS1
AHP terminations
ABF mean latitude (Jansen et al., 1996)
δ2H Alkane C29 GeoB 6518-1 (Schefuß et al., 2005)
δ18O Ruber GeoB 6518-1 (Schefuß et al., 2005)
Semi-quantitative Ti/Ca ratio
Terrigenous inputs
Tropical moisture
% Echinidinium spp.
Lingulodinium machaerophorum
% Stelladinium reidii*
% Operculodinium aguinawense*
% Brigantedinium spp.
Primary productivity
River discharges
% Selenopemphix nephroides*
% Spiniferites membranaceus*
% Spiniferites mirabilis*
% Operculodinium centrocarpum
This study
GeoB 1023 (Shi et al., 1998)
% Trinovantedinium applanatum
Trophic gradient (mesotrophic to eutrophic)
* : thermophiles species
Benguela advection
Upwelling activity
a1
a2
b1
b2
b3
c1
c2
Age ka cal. BP

Figure 8